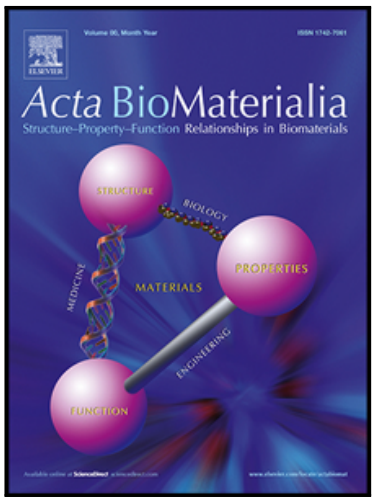


# Polyvinylidene fluoride-Hyaluronic acid wound dressing comprised of ionic liquids for controlled drug delivery and dual therapeutic behavior

Atiye Abednejad , Azadeh Ghaee , Eduarda S. Morais , Mukesh Sharma , Bruno M. Neves , Mara G. Freire , Jhamak Nourmohammadi , Ali Abouei Mehrizi

PII: S1742-7061(19)30674-9
DOI: https://doi.org/10.1016/j.actbio.2019.10.007
Reference: ACTBIO 6392

To appear in: *Acta Biomaterialia*

Received date: 13 May 2019
Revised date: 23 September 2019
Accepted date: 1 October 2019

Please cite this article as: Atiye Abednejad , Azadeh Ghaee , Eduarda S. Morais , Mukesh Sharma , Bruno M. Neves , Mara G. Freire , Jhamak Nourmohammadi , Ali Abouei Mehrizi , Polyvinylidene fluoride-Hyaluronic acid wound dressing comprised of ionic liquids for controlled drug delivery and dual therapeutic behavior, *Acta Biomaterialia* (2019), doi: https://doi.org/10.1016/j.actbio.2019.10.007

# Polyvinylidene fluoride-Hyaluronic acid wound dressing comprised of ionic liquids for controlled drug delivery and dual therapeutic behavior

**Atiye Abednejad[1], Azadeh Ghaee[1]*, Eduarda S. Morais[2], Mukesh Sharma[2], Bruno M. Neves[3], Mara G. Freire[2]*, Jhamak Nourmohammadi[1], Ali Abouei Mehrizi[1]**

[1] Department of Life Science Engineering, Faculty of New Sciences and Technologies, University of Tehran, P.O. Box: 143951374, Tehran, Iran

[2] CICECO-Aveiro Institute of Materials, Chemistry Department, University of Aveiro, Campus Universitário de Santiago, 3810-193 Aveiro, Portugal.

[3]Department of Medical Sciences and Institute of Biomedicine – iBiMED, University of Aveiro, 3810-193 Aveiro, Portugal

*Corresponding authors: Dr. Azadeh Ghaee, Email: ghaee@ut.ac.ir, and Dr. Mara G. Freire, Email: maragfreire@ua.pt.



## Statement of Significance

This work shows the preparation and characterization of bilayer wound dressings comprising dual-biological function active pharmaceutical ingredients based on ionic liquids with improved and controlled drug release and dual therapeutic efficiency. By converting analgesic and anti-inflammatory drugs into ionic liquids, their water solubility increases up to 470-fold. The prepared bilayer wound dressing membranes have desirable mechanical properties and improved release of drugs. The prepared membranes comprising ionic liquids display anti-inflammatory activity as effective as those with the original drugs. Cell adhesion of fibroblasts on membrane surfaces and cell viability assays show improved viability and adhesion of fibroblasts on PVDF/HA membranes, being thus of high relevance as effective transdermal drug delivery systems.

**Abstract**

To improve the efficacy of transdermal drug delivery systems, the physical and chemical properties of drugs need to be optimized to better penetrate into the stratum corneum and to better diffuse into the epidermis and dermis layers. Accordingly, dual-biological function ionic liquids composed of active pharmaceutical ingredients were synthesized, comprising both analgesic and anti-inflammatory properties, by combining a cation derived from lidocaine and anions derived from hydrophobic nonsteroidal anti-inflammatory drugs. Active pharmaceutical ingredient ionic liquids (API-ILs) were characterized through nuclear magnetic resonance, cytotoxicity assay, and water solubility assay. All properties were compared with those of the original drugs. By converting the analgesic and anti-inflammatory drugs into dual-function API-ILs, their water solubility increased up to 470-fold, without affecting their cytotoxic profile. These API-ILs were incorporated into a bilayer wound dressing composed of a hydrophobic polyvinylidene fluoride (PVDF) membrane to act as a drug reservoir and a biocompatible hyaluronic acid (HA) layer. The prepared bilayer wound dressing was characterized in terms of mechanical properties, membrane drug uptake and drug release behavior, and application in transdermal delivery, demonstrating to have desirable mechanical properties and improved release of API-ILs. The assessment of anti-inflammatory activity through the inhibition of LPS-induced production of nitric oxide and prostaglandin E2 by macrophages revealed that the prepared membranes containing API-ILs are as effective as the original drugs. Cell adhesion of fibroblasts on membrane surfaces and cell viability assay confirmed improved the viability and adhesion of fibroblasts on PVDF/HA membranes. Finally, wound healing assay performed with fibroblasts showed that the bilayer membranes containing dual-function API-ILs are not

detrimental to wound healing, while displaying increased and controlled drug delivery and dual therapeutic behavior.

**Keywords**: Active pharmaceutical ingredients; Ionic liquids; Dual function; Drug release; Polyvinylidene Fluoride; Hyaluronic acid; Bilayer wound dressing.

## 1. Introduction

Wound is defined as a condition in which the shape and the function of the skin are disrupted by any internal or external factor. Natural wound healing processes in the skin follow four phases: inflammation, proliferation, granulation, and tissue remodeling. In severe injuries, this natural process is neither sufficient nor effective [1]. Moreover, local factors such as lack of oxygenation and infection and systemic factors including age, stress, diseases like diabetes, and some medications might impair wound healing [2, 3]. Therefore, many studies have been investigating several approaches to improve wound healing, including skin grafts, biological- and biomaterial-based tissue engineering, and synthetic and natural wound dressings [4-7]. An ideal wound dressing must provide a moist environment, gas exchange, wound protection from infection, biocompatibility, and desirable mechanical properties as well as flexibility, natural healing stimulation, and antibacterial activity. Furthermore, the delivery of antibiotics, anti-inflammatory agents, and analgesics to the injured area should be accomplished [4-7].

Dressing systems with improved drug delivery abilities, such as microneedles, iontophoresis, matrix patches, and single-/multi-layer drugs in adhesives, have been proposed. One recent approach consists in reservoir-type wound dressings [8], which seem ideal for healing purposes because of their easy application on the skin; elimination of drug level fluctuation through steady, continuous, and controlled drug delivery; low demand for dressing renewal; and desirable

therapeutic efficacy [9]. One form of reservoir-type dressings corresponds to pore-filled membranes containing porous chemical and mechanically stable substrates filled with electrolytes, which, in addition to filtration and ion exchange applications, are also used in drug delivery [10].

To obtain reservoir-type wound dressings, synthetic polymers such as polypropylene (PP), polyethylene (PE), polyvinylpyrrolidone (PVP), polyvinyl alcohol (PVA), poly(lactic-co-glycolic acid) (PLGA), and polyvinylchloride (PVC) have been used [11,12]. Polyvinylidene fluoride (PVDF) is a chemically and thermally stable, hydrophobic polymer with high mechanical strength and piezoelectric properties and widely used in the biomedical field [13]. The internal porous structure of PVDF membranes makes them feasible as drug reservoirs, while their surface pores enable drug release. Although it is well established that synthetic polymers provide excellent mechanical properties, their low biocompatibility decreases cell adhesion, migration, and proliferation [14]. Many researchers have focused on the surface modification of synthetic polymers to improve their biocompatibility and cell viability. For instance, Gao *et al.* [15] used alginate to improve the biocompatibility of PVC, while Dubruel *et al.* [16] modified a polyimide (PI) surface with gelatin for the same purpose. In the same line, chitosan was applied to ameliorate cell adhesion on polylactic acid (PLLA) surfaces [17], whereas PEG modification was attempted to improve polyurethane (PU) biocompatibility [18].

Hyaluronic acid (HA) is a nonsulfated glycosaminoglycan (GAG) commonly used in biomedical applications [19, 20]. It is a biodegradable and biocompatible hydrogel-type polymer that naturally exists in the human cartilage and skin [21]. It has remarkable effects on skin cell proliferation, migration, and healing [22, 23]. On the basis of these advantages, Jayakumar e*t al.* [24] used HA and reported enhanced angiogenesis in wounds. Lin and co-workers [25] applied

HA for chronic wound and diabetic wound healing, while Matsumoto *et al.* [26] prepared wound dressings combining HA and arginine to improve healing.

Although HA can contribute to wound healing [27], it is essential to include the use of pharmaceuticals with antimicrobial, anti-inflammatory, and analgesic properties to increase the efficacy of wound dressings [28]. Nevertheless, low water solubility and low bioavailability are frequently experienced when applying such drugs directly in wound dressings. To overcome these limitations, commonly, highly hydrophobic drugs are converted to related salts and, more recently, to ionic liquids (ILs) [29]. Furthermore, therapeutic efficiency can be improved by combining APIs with different biological functions [30], which is a particular feature that can be accomplished with ILs.

ILs are organic salts, with melting points below 100˚C (by general definition) [31]. They are considered amorphous salts and do not have some of the limitations of crystalline salts, such as polymorphism. In addition to a wide range of applications in which they can be applied [32-34], in the last decade, ILs have received significant attention in the pharmaceutical field [35, 36] in the form of solvents to tailor polymorphism [37], solvents in drug synthesis and co-solvents to promote drug solubility [38], and in the design of APIs [39]. Furthermore, through appropriate selection of the IL anions and cations, API-ILs with dual biological effects can be produced [14].

In this work, a bilayer wound dressing material with controlled API-IL release capability was prepared. In particular, a PVDF membrane was used as the top layer to provide stability and act as the drug reservoir, while a HA hydrogel was used as the bottom layer to afford biocompatibility and additional healing features. Dual-biological function API-ILs with both analgesic and anti-inflammatory properties were synthesized; characterized in terms of purity, solubility, and cytotoxicity; and incorporated in the bilayer wound dressing material envisioning

wound healing The prepared membranes (with and without API-ILs) were characterized through Fourier transform-infrared spectroscopy (FT-IR), scanning electron microscopy (SEM), and mechanical property assays. Finally, drug uptake and release, transdermal delivery, cell adhesion, macrophage and fibroblast cell viability, and anti-inflammatory and wound healing assays were carried out. Similar assays for the original and salt-form drugs were performed for comparison purposes. Figure 1 summarizes the goal, steps, and investigations carried out in this work.

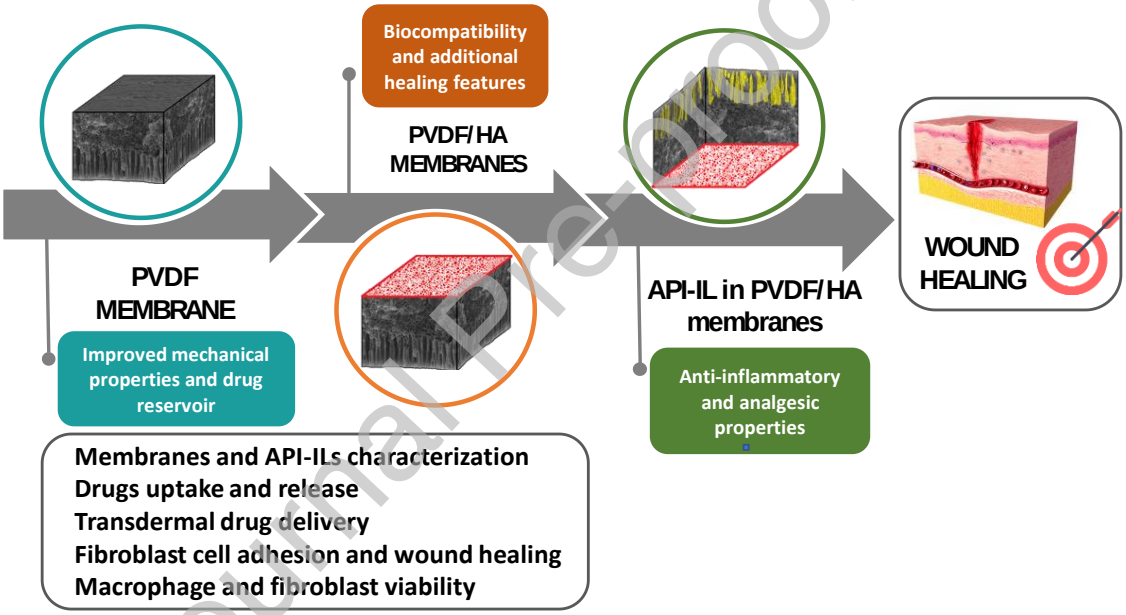


**Figure 1**. Conceptual summary of the goal, steps, and investigations carried out in the current work.

## 2. Materials and methods

### 2.1 Materials

PVDF polymer powder (Kynar 740, high purity) was obtained from Arkema, Philadelphia, USA. Dimethylacetamide (DMAC) (99% purity) and chloroform (>99% purity) were provided by Fisher Chemical (USA) and Carlo Erba (France), respectively. N-hydroxysuccinimide (NHS) (98% purity), 1-ethyl-3-(3-dimethylaminopropyl) carbodiimide hydrochloride (EDC) (98%

purity), dopamine, and phosphate buffer solution (PBS) were purchased from Sigma-Aldrich, while HA sodium salt (medical grade, 1000 kDa, >95% purity, viscosity = 2.05 $m^3$/kg) was supplied by APRIN Biomedical Ltd. Sodium diclofenac, sodium ibuprofen (>98% purity), sodium naproxen (98% purity), and lidocaine.HCl (>96% purity) were purchased from Sigma-Aldrich, Acros Organics, and Iran Darou Pakhsh Chemical Pharmaceutical Company, respectively. Noncharged nonsteroidal anti-inflammatory drugs (NSAIDs) including ibuprofen, naproxen, and diclofenac were provided by Sigma-Aldrich. L929 fibroblast cell line was provided by the Pasteur Institute of Iran, whereas Raw 264.7 macrophages (TIB-71) and 3T3 mouse fibroblasts (CRL1658) were acquired from American Type Culture Collection, Manassas, USA. Dulbecco's modified Eagle's medium (DMEM) cell culture medium, dimethyl sulfoxide (DMSO), and fetal bovine serum (FBS) were obtained from Sigma, USA. Dermatomed excised human skin from plastic surgery was provided by Center for Research and Training in Skin Diseases and Leprosy, Iran.

### 2.2 Methods

#### 2.2.1 Synthesis of dual-biological (anti-inflammatory and analgesic) function API-ILs and their characterization

The prepared API-ILs contain the charged form of lidocaine as a cation, providing analgesic features, and negatively charged NSAIDs (derived from ibuprofen, diclofenac, and naproxen) as anions, with anti-inflammatory properties. API-ILs were synthesized by the reaction of lidocaine.HCl with the sodium salts of each NSAID, namely, sodium ibuprofen, sodium diclofenac, and sodium naproxen following a previously reported protocol [40]. Briefly, equimolar quantities of lidocaine.HCl and each NSAID sodium salt were dissolved in deionized water and mixed under continuous stirring for 1 h at 80°C. The solution was then cooled down to

room temperature and extracted in chloroform to remove the produced sodium chloride (NaCl) salt. API-ILs, namely, Lidocainium Naproxenum ([Lido][Nap]), Lidocainium Ibuprofenate ([Lido][Ibu]), and Lidocainium Diclofenac ([Lido][Diclo]), were washed with water three times and left under reduced pressure to remove residual volatile solvents. To confirm the complete reaction and NaCl elimination, the chloride content in each API-IL was determined with a $Cl^-$-selective Metrohm electrode, using TISAB solutions of $NaNO_3$ [41]. NaCl was used to obtain the calibration curve. The average number of moles of $Cl^-$ *per* mole of each API-IL was found to be below 2%, confirming that the reaction was complete. The chemical structures of the prepared API-ILs were confirmed by $^1H$ and $^{13}C$ NMR spectroscopy and elemental analysis. NMR spectra were recorded using a Bruker Avance 300 (France) at 300.13 MHz, using dimethyl sulfoxide (DMSO) as solvent and tetramethylsilane (TMS) as internal reference. Elemental analyses (C, H, and N) of all synthesized ILs were carried on a PerkinElmer 2400 C, H, and N element analyzer. Thermogravimetric analysis (TGA) was used to determine the decomposition temperature ($T_{dec}$) of API-ILs using a Setsys Evolution 1750 (SETARAM) instrument. Samples were heated at a temperature range of 25-800°C in an aluminum pan under nitrogen atmosphere, with a heating rate of 10°C.min$^{-1}$. A power compensation differential scanning calorimeter (Hitachi DSC7000X DSC, Japan) was used to determine the melting temperature ($T_m$) and glass transition temperature ($T_g$) of API-ILs in hermetically sealed aluminum crucibles under constant nitrogen flow (50 mL.min$^{-1}$). Twenty milligrams of each sample was used to determine the temperature and enthalpy of fusion at a scanning rate of 5 K.min$^{-1}$ under constant nitrogen flow. Each TGA and DSC analysis was repeated five times.

Saturated aqueous solutions of dual-biological function API-ILs and their corresponding drugs, namely, the original drugs with no counter-ions and the respective sodium salts, were prepared to

determine their water solubility. API-ILs and the remaining drugs were added in excess to 1 mL of water and dissolved at constant temperature and agitation (37ºC, 750 rpm) for 72 h using an Eppendorf ThermoMixer Comfort. After reaching equilibrium, the samples were centrifuged at 4500 rpm for 20 min using a Hettich Mikro-120 centrifuge. The samples were then placed in an air bath equipped with a Pt 100 probe and a PID controller at 37°C for 2 h. Aqueous samples were then carefully collected and diluted in ultrapure water to quantify each drug, namelythe noncharged drugs, the NSAID sodium salts, and dual-biological function API-ILs. The analytical techniques used to quantify each drug were UV spectroscopy, using a Shimadzu UV-1700 spectrophotometer, and high-performance liquid chromatography, using a Shimadzu PROMINENCE, an analytical C18 reversed-phase column (250 × 4.60 mm), and kinetex 5-µm C18 100 A column from Phenomenex along with a DAD detector (HPLC-DAD). The HPLC mobile phase included 40% (v:v) of PBS at pH 6.5 and 60% (v:v) of acetonitrile, with an injection volume of 10 µL at a flow rate of 1 $mL.min^{-1}$ [42]. The column oven and autosampler were operated at a constant temperature (30°C). Saturation was determined at $\lambda_{max}$ using previously established calibration curves for each API, API sodium salt, and API-IL. In the case of API-ILs, both the cation and the anion were quantified. Each experiment was replicated five times, and the data given correspond to the average value ± standard deviation [43].

**2.2.2 Preparation of PVDF flat sheet membranes and HA grafting**

PVDF membranes were prepared according to a previously reported method [44]. DMAC was chosen as the solvent because of the formation of specific structures in PVDF membranes that seem ideal for reservoir applications. Briefly, 18, 22, 26, and 30 wt.% PVDF was dissolved in DMAC by stirring at 50°C for 24 h. After degassing in an ultrasonic bath for 90 min and resting for 24 h, PVDF casts were spread on a glass surface using a film applicator and immersed in

20°C water for phase inversion and membrane formation. To remove the solvent, membranes were kept in distilled water for 48 h. To prepare the HA solution, 0.1 g of HA was dissolved in 10 mL deionized water (1 wt.% solution of HA) and stirred overnight at room temperature. EDC/NHS (100 mM/100 mM) was then added to 5 mL ethanol and mixed for 1 h to dissolve. To crosslink the HA hydrogel, the EDC/NHS/ethanol solution was added to the HA solution at an acidic pH (4.5-5.0) and stirred for 12 h [45]. It should be remarked that ethanol has a low vapor pressure and provides a slightly acidic environment, leading to faster HA crosslinking and drying, as demonstrated in the literature [45-48].

To provide bilayer wound dressing, the PVDF membrane surface was first activated by wet chemistry using dopamine following a previously reported protocol [49]. PVDF membranes were immersed in 1 g/L dopamine-PBS solution for 10 h. Membranes were taken out and washed with deionized water and finally covered with the HA hydrogel.

**2.2.3 API impregnation into PVDF membrane pores**

To impregnate the original drugs and the dual-biological function API-ILs into PVDF membrane pores, aqueous solutions containing each API and API-ILs, at values close to their saturation, were placed in equilibrium at the unmodified side of the PVDF membranes for 24 h. Finally, the membranes were taken out and dried at 40°C for 24 h.

**2.2.4 Membrane characterization**

A scanning electron microscope (SEM) (S-4100 Hitachi, Japan (20 Kv)) was used to study the membrane morphology (surface and cross sections). To obtain membrane cross sections, the samples were broken in liquid nitrogen. All samples were coated with gold before imaging. Chemical compositions of the prepared membranes before and after HA grafting were characterized by ATR-FTIR (Fourier transform infrared) with 4 $cm^{-1}$ resolution at a range of

400-4000 $cm^{-1}$ using an FTIR Bruker Tensor 27, Germany. An INSTRON 5966 dynamic testing equipment equipped with a data acquisition system was used to perform tensile testing. The gauge length and cross-head speed were 50 mm and 10 mm/min, respectively. Tensile tests were performed according to ASTM D882 standard with tension load cell to investigate the mechanical properties of the membranes. These assays were carried out at least 5 times for each sample.

To evaluate the API uptake of the PVDF and PVDF/HA membranes, the membranes were weighed before immersion in PBS aqueous solutions of APIs and API-ILs and after drying. The API uptake percentage was determined using the following equation:

$$API\ Uptake(\%) = [(Wf - Wi)/Wi] \times 100 \quad (1)$$

where $W_i$ and $W_f$ are the initial and final membrane weights, respectively.

The release of API-ILs and API sodium salts from the PVDF and PVDF/HA membranes was determined by the Franz cell method [50]. Solutions of saturated API-ILs and API sodium salts, namely, [Lido][Diclo], [Lido][Ibu], [Lido][Nap], lidocaine.HCl, sodium naproxen, sodium diclofenac, and sodium ibuprofen, were prepared. PVDF and PVDF/HA membranes loaded with APIs and API-ILs were trimmed into circular discs to cover the diffusion area of the Franz cell receptor. The membranes were then positioned between the donor compartment and the receiver compartment and occluded with paraffin to avoid evaporation [51]. The samples were taken out after 1, 2, 4, 6, 8, 12, 24, 48, 72, 96, and 120 h, and the drugs were quantified by UV and HPLC-DAD using established calibration curves as previously described. Sample volumes were replaced with equal volumes of fresh PBS aqueous solution (NaCl: 0.137 M, KCl: 0.0027 M, $Na_2HPO_4$: 0.01 M, $KH_2PO_4$: 0.0018 M; pH ~7.4). Cumulative percentages of released APIs were

calculated. Each experiment was replicated five times, and the data provided correspond to the average value ± standard deviation.

To investigate the transdermal delivery and permeation of APIs and API-ILs into the skin, the Franz-type diffusion cell was used as described in the literature [51-54]. Although the general procedure is similar to the described release study procedure, the dermatomed human skin excised from plastic surgery was positioned under the PVDF/HA membranes loaded with APIs and API-ILs, between the donor compartment and the receiver compartment as described in the literature [55, 56]. Cumulative percentages of released drugs were calculated.

**2.2.5 Biological Assays**

**2.2.5.1 Cell adhesion onto PVDF and PVDF/HA membranes**

To investigate the adhesion of fibroblast cells on PVDF and PVDF/HA membrane surfaces (unloaded and API-IL-loaded membranes), the cells were cultured for 2 days. Culture media contained DMEM (low glucose; Sigma, USA), 10% (v:v) FBS (Sigma, USA), 1% (v:v) Pen-Strep (100 U/ml penicillin and 100 µg/ml streptomycin; Sigma–Aldrich, USA). Five-millimeter-diameter samples were sterilized by immersion in 70% ethanol for 1 h at room temperature and rinsed with PBS. The samples were placed into a 96-well cell culture plate, and cells were seeded at a density of $10^4$ cells/well. The samples were incubated in 5% $CO_2$ atmosphere at 37°C for 24 h. For fibroblast cell fixation, after washing the cells with PBS (pH 7.4) aqueous solutions three times, the HA and PVDF/HA samples were immersed in 4.5% (v:v) glutaraldehyde/PBS solutions for 2 h. Finally, the samples were dehydrated stepwise in series of ethanol/PBS solutions (30-100%, each step for 10 min) and dried overnight. The membrane surface was morphologically characterized by SEM as described before.

**2.2.5.2 Viability assays**

The resazurin assay was used to assess the effect of the APIs, API-ILs, and PVDF/HA membranes loaded with API-ILs on macrophage viability [57]. Briefly, $1.5 \times 10^6$ Raw 264.7 cells per well were cultured in a 6-well plate and left to stabilize overnight. For assays with membranes, the samples were placed in contact with cell cultures for 24 h by means of 24 mm Transwell inserts with 0.4 μM polycarbonate membranes (Corning, NY, USA). Resazurin was added to cells at a final concentration of 50 μM during the last 1 h of incubation. Finally, 200 μL from each condition was transferred to a 96-well plate, and the absorbance of the product of the resazurin reduction was measured at 570 and 600 nm in a Bio-Tek Synergy HT spectrophotometer (Bio-Tek Instruments, Winooski, VT, USA).

Fibroblast viability was also evaluated for APIs, API-ILs, PVDF, and PVDF/HA membranes loaded with API-ILs by the MTT assay. First-cultured L929 fibroblast cells were seeded on sterilized membranes positioned in a 48-well plate ($2 \times 10^5$ cells/well) and kept in a $CO_2$ incubator (5% $CO_2$ at 37 °C) for 24 h (Stat Fax 2100; GMI, USA). Then, the culture medium was removed after 24 h and refreshed by 10 μL MTT solution (5 mg/mL). After 4 h, 50 μL DMSO was added to each well to dissolve formed formazan crystals. Absorbance was detected at 545 nm using an ELISA microplate reader (Stat Fax 2100, USA) [58].

The given data are the average of at least five biological independent experiments conducted in duplicate for each condition, whose results are expressed as the average cell viability ± standard deviation. Membranes were sterilized at 121ºC in an autoclave before viability tests.

**2.2.5.3 Anti-inflammatory assays**

The potential anti-inflammatory activities of APIs and the bilayers membranes containing APIs were tested by analyzing their capacities to inhibit LPS-induced nitric oxide (NO) and prostaglandin E2 production in macrophages. Raw 264.7 cells were plated at a density of $3 \times 10^5$

cells/well in a 48-well culture plates, allowed to stabilize for 12 h, and then incubated with culture medium (control), APIs, and PVDF/HA membranes loaded with API-ILs for 24 h. For NO quantification, at the end of the incubation, 100 µL of culture supernatants was collected and mixed with an equal volume of Griess reagent [0.1% (w/v) N-(1-naphthyl)ethylenediamine dihydrochloride and 1% (w/v) sulfanilamide containing 5% (w/v) $H_3PO_4$] for 30 min in the dark. After 30 min incubation in the dark, the absorbance at 550 nm was measured using a standard spectrophotometer Bio-Tek Synergy HT (Bio-Tek Instruments, Winooski, VT, USA). Prostaglandin E2 was quantified in cell supernatants using an ELISA kit according to the manufacturer's instructions (R&D Systems, Minneapolis, USA).

**2.2.5.4. Wound healing assays**

The effects of PVDF and PVDF/HA membranes loaded with API-ILs on the spreading and migration capabilities of 3T3 fibroblasts were assessed using a scratch wound assay, which addresses the expansion of a cell population on surfaces. The cells were seeded in a 12-well tissue culture dishes at a concentration of $3\times10^5$ cells/mL and left in a medium containing 10% FBS until they nearly reached a confluent cell monolayer. Then, a linear wound was generated in the monolayer with a sterile 200 µL plastic pipette tip. Any cellular debris was removed by washing the coverslips with PBS. At least five images of the scratched area of each condition were taken at the 0 h time point using an Evos M5000 Cell Imaging System (Thermo Fisher Scientific, Massachusetts, USA) at 4× magnification. Tested stimuli were added in medium containing 2% FBS. Media containing 10% FBS and *Cytochalasin* D were used as positive and negative controls, respectively. After 16 h, at least five images of the scratched area of each condition were taken and compared to the corresponding 0 h time point.

### 2.2.6 Statistical analysis

Each experiment was conducted 3 to 5 times, and the results are reported as average ± standard deviation. Unless otherwise stated, one-way analysis of variance (ANOVA) with Dunnett´s multiple comparison post-hoc test was used to appraise the significance of the data, and $p < 0.05$ was considered as significant [59]. Statistical analysis was performed using GraphPad Prism, version 6 (GraphPad Software, San Diego, CA, USA).

## 3. Results and discussion

### 3.1 API-IL synthesis and characterization

Dual-biological function API-ILs, namely, [Lido][Diclo], [Lido][Ibu], and [Lido][Nap], were synthesized and characterized. Their chemical structure and macroscopic appearance at room temperature are shown in Figure 2. All API-ILs were initially characterized by NMR and elemental analysis, and these results are given in Supplementary Information (Figures S1 and S2; Table S1).

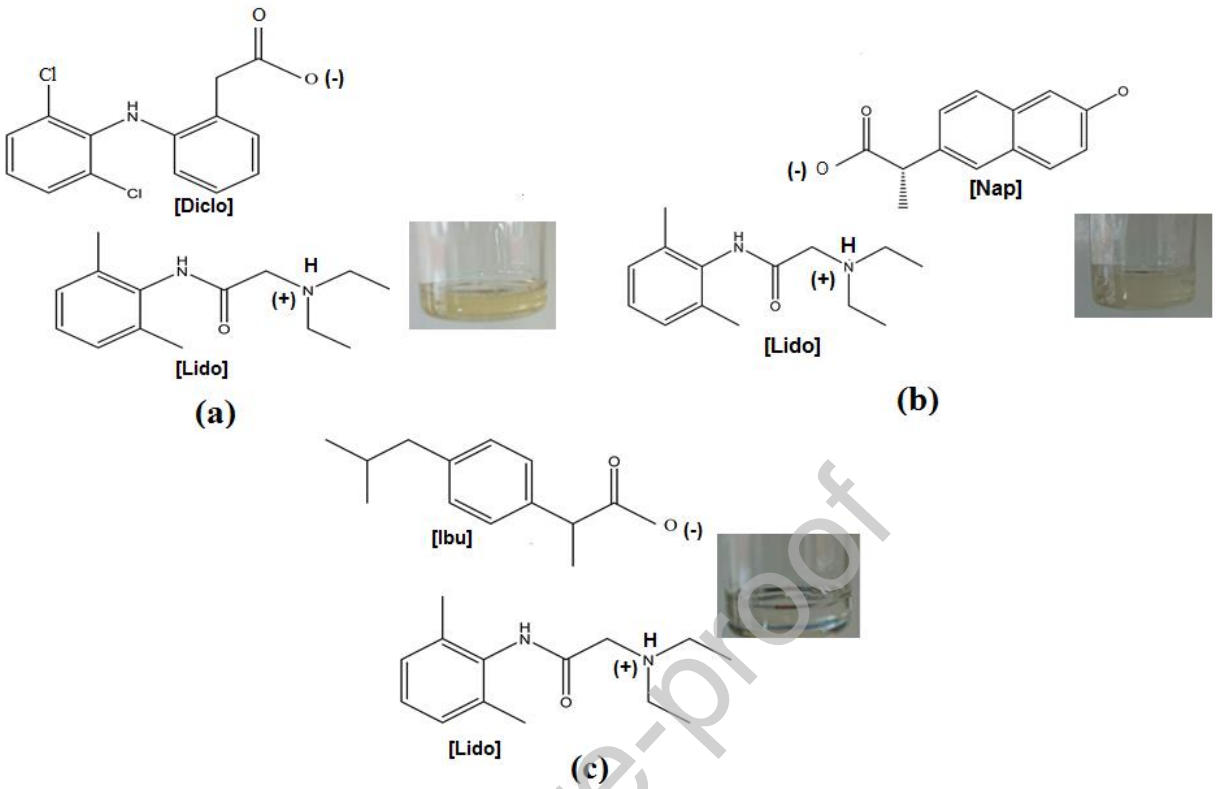


**Figure 2.** Chemical structure and macroscopic appearance of (a) [Lido][Diclo], (b) [Lido][Nap], and (c) [Lido][Ibu] at room temperature

As shown in Figure 2, all ILs are liquid at room temperature, fitting within the room-temperature IL class. To the best of our knowledge, the synthesis of [Lido][Ibu] has already been reported in the literature [40], whereas the preparation of [Lido][Diclo] and [Lido][Nap] is reported here for the first time. Thermal properties, namely, melting temperature ($T_m$), glass transition temperature ($T_g$), and decomposition temperature ($T_{dec}$), of the dual-biological function API-ILs were determined by differential scanning calorimetry (DSC) and thermogravimetric analysis (TGA). Their thermal behavior is shown in Supplementary Information (Figure S3). According to the melting temperature and glass transition temperature given in Table 1, it is confirmed that the prepared API-ILs present melting temperatures between 11.0 and 37 ºC, being liquid at room

temperature. This is an important advantage when foreseeing their therapeutic application by their incorporation into membranes and improved bioavailability.

The incorporation of a cation derived from lidocaine significantly decreases the melting temperature of API-ILs when compared with that of the respective drugs and sodium salts. The $T_{dec}$ values listed in Table 1 demonstrate that the synthesized dual-biological function API-ILs, namely, [Lido][Ibu], [Lido][Diclo], and [Lido][Nap], present high thermal stability: 228, 255, and 234 ºC, respectively. Among the prepared API-ILs, [Lido][Diclo] has the highest thermal stability. These values are similar and even higher in some examples when compared with the values of the original noncharged drugs and respective sodium salts, as reported in the literature [60-70], and are given in Table 1.

**Table 1.** Thermal properties (decomposition, melting, and glass transition temperatures) of dual-biological function API-ILs, API sodium salts, and noncharged APIs.

| | | $T_{dec}$ (± 1 °C) | $T_m$ (±0.5 °C) | $T_g$ (±0.5 °C) | Reference |
|---|---|---|---|---|---|
| API-ILs | [Lido][Ibu] | 228 | 11.0 | -37.2 | ---[a] |
| | [Lido][Nap] | 234 | 22.8 | -33.1 | ---[a] |
| | [Lido][Diclo] | 255 | 37.0 | -3.32 | ---[a] |
| API sodium salts | Lidocaine.HCl | - | 74-79 | - | [60] |
| | Ibuprofen.Na | 222 | 220 | - | [60, 61] |
| | Naproxen.Na | 244-246 | 244-262 | - | [62, 63] |
| | Diclofenac.Na | 270-390 | 285 | - | [64, 65] |
| Noncharged APIs | Lidocaine | - | 68 | - | [66] |
| | Ibuprofen | 282 | 75-77 | - | [67] |
| | Naproxen | 196-200 | 158 | - | [68] |
| | Diclofenac | 185 | 156-158 | - | [69, 70] |

[a]Experimentally determined in the work

As the water solubility of drugs significantly affects their bioavailability, the water solubility of the dual-biological function API-ILs was determined and compared with the corresponding APIs and API sodium salts at 37 °C. The solubility data and the respective standard deviations are reported in Table 2. For API-ILs, both the cation and anion of IL were quantified, and the given results are an average of both quantifications. Detailed data per ion are given in the Supplementary Information (Table S2). Although some debate may exist on this fact [71], we demonstrate here that there is a close equimolar solubility of dual-biological function API-IL ions, guaranteeing a homogeneous solubility of both APIs and possible dual therapeutic efficiency.

Solubility results confirm that the water solubility of API-ILs is significantly higher than the water solubility of the original APIs, except for the API-IL [Lido][Diclo] that has a lower water solubility than lidocaine, which is also a result of the low solubility of diclofenac that is among

the less soluble NSAIDs studied. Overall, the solubility of API-ILs follows the trend of the respective noncharged NSAIDs, which usually display low solubility in water because of the large hydrophobic groups in their structure [72].

The solubility of lidocaine at 37 ºC is 0.017 mmol.mL$^{-1}$, whereas the solubility of the noncharged NSAIDs ranges between $8\times10^{-6}$ and $4.5\times10^{-4}$ mmol.mL$^{-1}$. When these NSAIDs are converted to sodium salts, solubility values from 0.027 to 1.96 mmol.mL$^{-1}$ are obtained. By converting these APIs into dual-function API-ILs, solubility values range between 0.0038 and 0.045 mmol.mL$^{-1}$, with an increase up to 470-fold when compared with the noncharged NSAIDs. In general, API-ILs are less water soluble than the respective sodium salts as a result of replacing the high-charge density sodium ion by a large organic cation derived from lidocaine. Yet, these API-ILs have the advantages of being liquid at room temperature and human body temperature and providing dual therapeutic efficiency.

Thermal behavior data confirm that the prepared dual-function API-ILs are liquid at room temperature and thus avoid typical problems of solid state drugs, such as polymorphism, whereas solubility results demonstrate an enhanced water solubility that is beneficial to improve bioavailability. Although decreases in the water solubility were observed for some dual-biological function API-ILs [68], in this work, we observed a general improvement in the water solubility with the prepared dual-biological function API-ILs comprising both analgesic and anti-inflammatory properties.

**Table 2.** Water solubility of dual-biological function API-ILs, API sodium salts, and noncharged APIs ($mmoL.mL^{-1}$) at 37 ºC.

| | | **Solubility ± σ ($mmoL.mL^{-1}$)** |
|---|---|---|
| API-ILs | [Lido][Ibu] | $(4.18 \pm 0.06) \times 10^{-2}$ |
| | [Lido][Nap] | $(3.79 \pm 0.03) \times 10^{-2}$ |
| | [Lido][Diclo] | $(3.81 \pm 0.01) \times 10^{-3}$ |
| API sodium salts | Lidocaine.HCl | 1.96 ± 0.07 |
| | Ibuprofen.Na | $(7.51 \pm 0.06) \times 10^{-1}$ |
| | Naproxen.Na | $(3.63 \pm 0.01) \times 10^{-1}$ |
| | Diclofenac.Na | $(2.76 \pm 0.02) \times 10^{-2}$ |
| Noncharged APIs | Lidocaine | $(1.7 \pm 0.1) \times 10^{-2}$ |
| | Ibuprofen | $(4.51 \pm 0.02) \times 10^{-4}$ |
| | Naproxen | $(2.64 \pm 0.01) \times 10^{-4}$ |
| | Diclofenac | $(8.1 \pm 0.1) \times 10^{-6}$ |

### 3.2 Membrane characterization

#### 3.2.1 Pristine PVDF membranes

Figure 3 shows the morphology of PVDF membranes with 18, 22, 26, and 30 wt.% polymer concentrations prepared using DMAC as solvent at 20 °C. The increase in the PVDF concentration leads to a spongy region formation, consistent with the findings reported in literature [73]; this behavior could be attributed to the presence of more polymeric chains and higher viscosity. Finger-like structures enable the membrane to hold APIs, while the spongy region plays an important role in API release, as it controls the passage of the drug through the pores. At 18 wt.% PVDF concentration, a more porous structure with larger pore diameters is

obtained, which would not be suitable to hold APIs and could result in a burst release. On the other hand, at 26 and 30 wt. % PVDF concentration, spongy regions with smaller pore diameters are dominant. It is, however, difficult to distinguish finger-like structures from spongy regions in membranes with 30 wt.% PVDF. Thick spongy regions would increase the time required for IL transfer by limiting diffusion; thus, 22 wt.% seems to be the ideal PVDF concentration for the envisioning application.

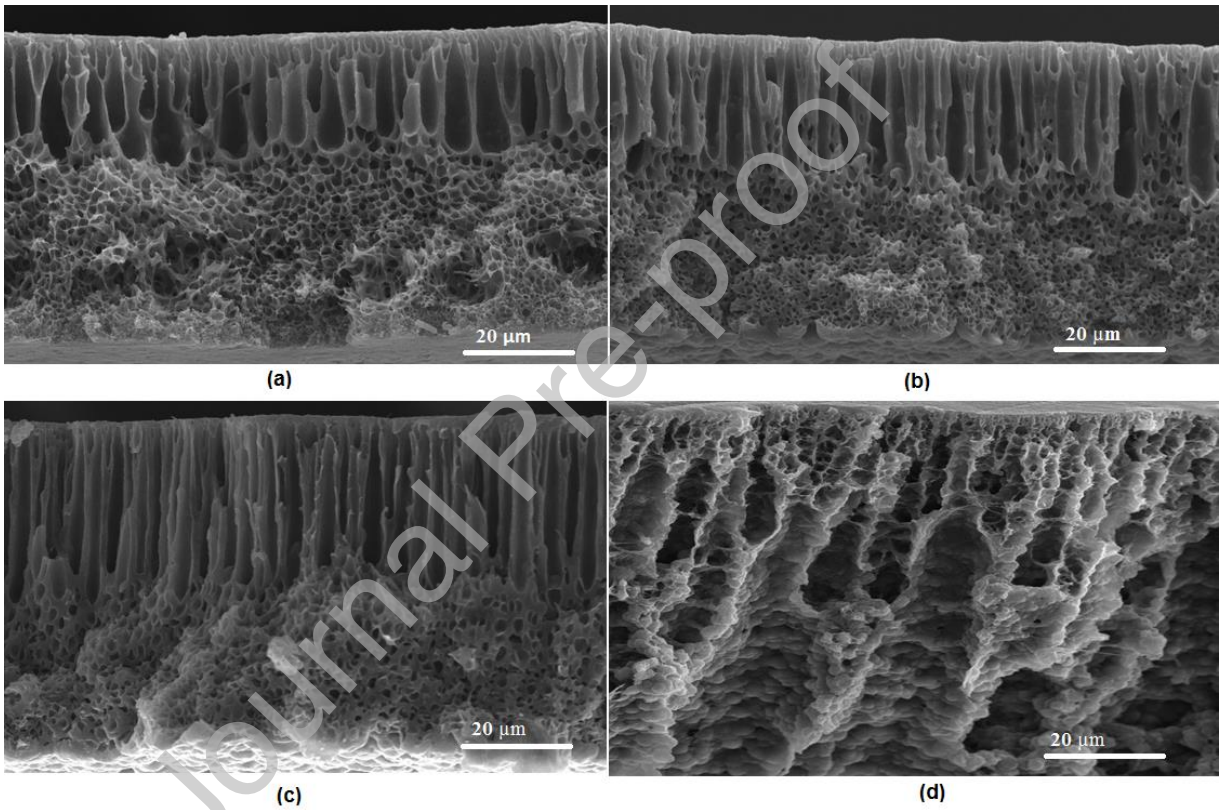


**Figure 3.** SEM images of PVDF membrane cross sections at (a) 18 wt.% PVDF, (b) 22 wt.% PVDF, (c) 26 wt.% PVDF, and (d) 30 wt.% PVDF. The scale bars correspond to 20 µm.

As the PVDF membrane layer is incorporated to provide mechanical stability to the bilayer wound dressing, its mechanical properties have been investigated through tensile tests. The effect of PVDF concentration on the mechanical properties of the membranes, namely, Young's

modulus (E), tensile strength (σ), and elongation at break (ε), is shown in Table 3 and Figure S4 in Supporting Information. As the percentage of PVDF increases from 18 to 30 wt.%, the Young's modulus (E) increases, while the elongation at break declines. This behavior confirms the improvement of mechanical strength because of the brittle behavior and a decline in the PVDF membrane flexibility. These results are a result of the nature of the polymeric chains in PVDF: as the concentration of PVDF increases, the viscosity of the polymeric solution and the density of polymeric chains increase, resulting in a higher Young's modulus and linear stress-strain behavior [73].

### 3.2.2 PVDF/HA membranes

To promote a desirable morphological structure and API-IL release, HA was grafted on the 22 wt.% PVDF membrane surface. Figure 4 depicts SEM images of PVDF and PVDF/HA membrane surfaces. Fewer and smaller surface pores can be observed after grafting HA on PVDF, which can restrict burst release of drugs from the PVDF membrane and thus lead to a controlled release of the drugs.

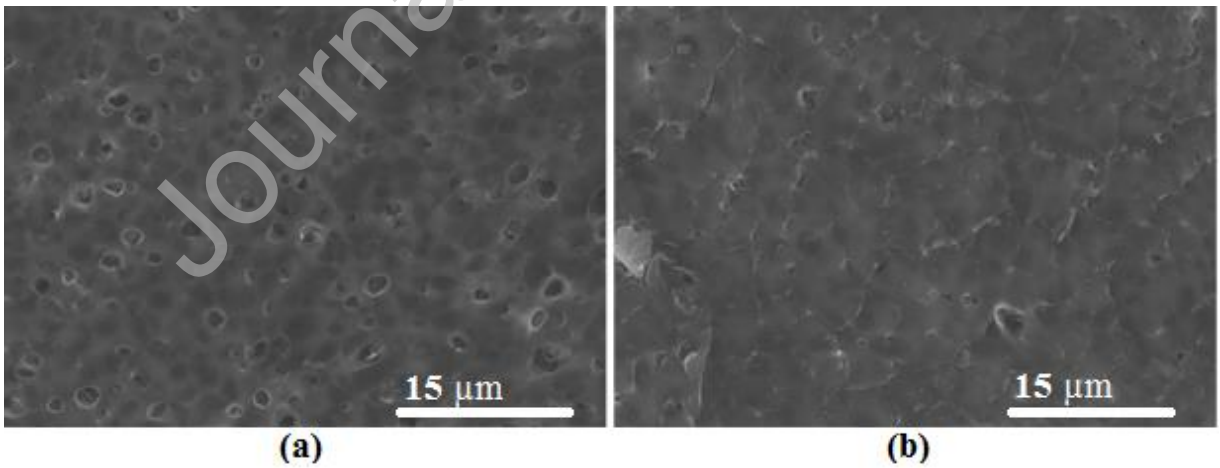


**Figure 4.** SEM images of the (a) PVDF surface and (b) PVDF/HA surface. The scale bars correspond to 15 µm.

ATR-FTIR spectra of PVDF, HA, and PVDF/HA membranes are shown in Figure 5. For the PVDF membrane sample, the bands at 873 and 1401 $cm^{-1}$ are attributed to C-F vibration, while the 1177 $cm^{-1}$ peak is related to the symmetrical stretching of the $–CF_2$ groups [74, 75]. Furthermore, the peaks at 840 and 1067 $cm^{-1}$ correspond to stretching in the ß phase, whereas the peak at 762 $cm^{-1}$ is assigned to in-plane bending in the α phase of PVDF [76, 77]. The spectrum related to HA shows peaks at 900–1200 $cm^{-1}$, which correspond to the O-C-O glycosidic bond of polysaccharides [14]. Peaks at 1541, 1661, and 1733 $cm^{-1}$ are assigned to the amide I, II, and C=O, respectively [45]. The stretching vibration peaks at 3334 and 2976 $cm^{-1}$ correspond to the hydroxyl and methylene groups of HA, respectively [58]. The ATR-FTIR spectrum of PVDF/HA is shown in Figure 5. The corresponding peaks of PVDF (762, 838, 873, 1070, and 1182 $cm^{-1}$) and HA (1541, 1661, 2976, and 3334 $cm^{-1}$) are presented, demonstrating the presence of both PVDF and HA. Peaks at 1733 and 1773 $cm^{-1}$, attributed to the carbonyl group, indicate a shift to 1712 and 1753 $cm^{-1}$, respectively. These peak shifts confirm the conjugation between HA and dopamine-activated PVDF [78]. Dopamine contains active functional groups including hydroxyl and amine, and it has been shown that dopamine can bind to PVDF by C-N bond formation [79]. As dopamine exists on the PVDF membrane surface, it would interact with HA through hydrogen bond formation [80].

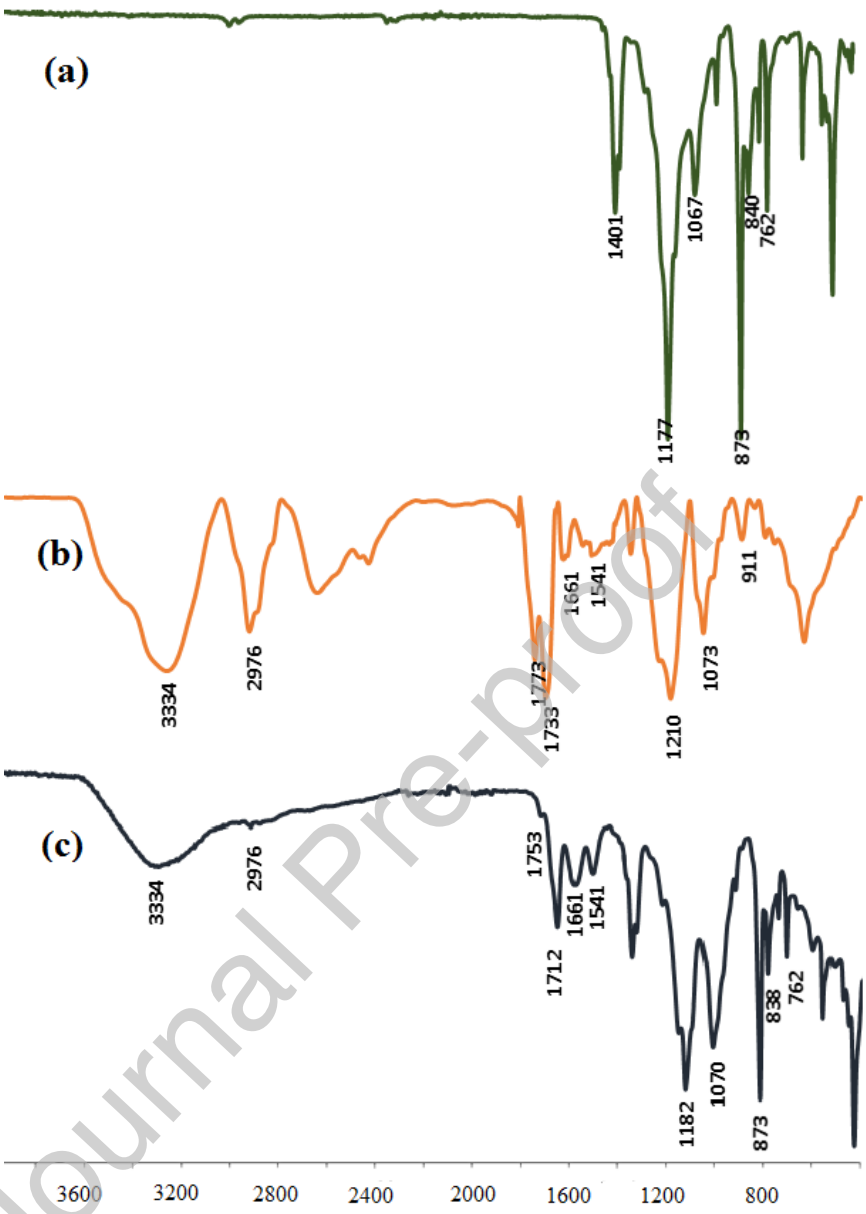


**Figure 5.** ATR-FTIR spectra of (a) PVDF, (b) HA, and (c) PVDF/HA.

As the hydrophilic layer of wound dressing would be in direct contact with the wound and it would swell and experience changes in mechanical properties, tensile tests were carried out on dry and swollen HA alone and after grafting on PVDF membranes (results given in Figure S5 of the Supplementary Information). Table 3 demonstrates the mechanical properties of dry and

swollen HA. The gathered results reveal that the mechanical strengths of HA under dry and swollen conditions are not similar. As HA swells, both Young's modulus and elongation at break decrease significantly (0.05 MPa and 3.22%, respectively). This reduction is explained by the fact that as water molecules penetrate in the HA structure and cause swelling, disentanglement of the polymer chains occurs, leading to a decrease in mechanical strength and lower required force for elongation [81]. Mechanical properties of PVDF/HA membranes were also evaluated before and after swelling. The mechanical properties of PVDF/HA membranes do not present significant changes before and after HA swelling, confirming that the PVDF layer prevents changes in the mechanical properties of HA after swelling. This characteristic guarantees the stability of the dressing while in contact with the wound.

**Table 3.** Mechanical properties (elongation at break, Young's modulus, and tensile strength at yield) of PVDF, HA, and PVDF/HA membranes.

| **Properties** | **Elongation at Break (%)** | **Young's Modulus (MPa)** | **Tensile strength at yield (MPa)** |
|---|---|---|---|
| PVDF (18 wt.%) | 11.7 ± 0.4 | 44.3 ± 0.1 | 1.1 ± 0.2 |
| PVDF (22 wt.%) | 8.2 ± 0.3 | 56.7 ± 0.5 | 1.6 ± 0.4 |
| PVDF (26 wt.%) | 6.3 ± 0.6 | 74.8 ± 0.8 | 2.2 ± 0.5 |
| PVDF (30 wt.%) | 2.4 ± 0.1 | 135.7 ± 0.5 | 3.2 ± 0.3 |
| HA | 17.5 ± 0.9 | 0.10 ± 0.01 | 0.72 ± 0.03 |
| Swollen HA | 3.2 ± 0.3 | 0.053 ± 0.003 | 0.23 ± 0.01 |
| PVDF (22 wt.%)/HA | 10.5 ± 0.2 | 62.5 ± 0.4 | 1.7 ± 0.3 |
| PVDF/Swollen HA | 9.5 ± 0.8 | 60.2 ± 0.3 | 1.65 ± 0.06 |

### 3.2.3 API membrane uptake and release

The API uptake percentage by PVDF membranes (18, 22, 26, and 30% PVDF) is presented in Table S4 of the Supplementary Information. These results reveal that the shape, size, and

interconnectivity of pores affect the membrane uptake of APIs and API-ILs. The highest uptake, that is, 16.7%, was observed with the 22 wt.% PVDF membranes. Structures with larger pores are desirable for reservoir applications, but the exodus of ILs from larger pores is faster. Accordingly, there is a decrease in the uptake percentage of 18 wt.% PVDF membranes (13.2%). In 26 and 30 wt.% PVDF membranes, the drug uptake decreases to 12.1% and 9.7%, respectively, which can be attributed to a decline in the porosity of the membranes. As the polymeric region increases in the membranes, free space available for holding ILs is diminished.

The PVDF membrane layer was intended to act as a drug reservoir; therefore, PVDF at 22 wt.% concentration was considered as the ideal choice, as it provides mechanical strength and relative flexibility as well as desirable API-IL uptake. The uptake of different API-ILs, corresponding APIs, and API sodium salts was determined. A high PVDF membrane uptake capacity for NSAIDs and NSAID salts was observed, while this parameter is low for lidocaine and lidocaine.HCl (Table 4). This phenomenon can be explained by capillary forces that are influenced by the hydrophobic–hydrophilic interactions occurring between drugs and the PVDF membrane [82]. As NSAIDs have a more hydrophobic behavior, their tendency to be incorporated into PVDF pores is higher [83]. On the other hand, lidocaine and lidocaine.HCl are more hydrophilic drugs than NSAIDs and NSAIDs salts, and thus, their penetration into membrane pores is more limited [84]. The uptake for NSAID salts is slightly lower than that for NSAIDs, which can be attributed to their more hydrophilic behavior.

The uptake by the 22 wt.% PVDF membrane for API-ILs is shown in Table 4. Results demonstrate that the membrane uptake capacity for API-ILs is higher than that for lidocaine.HCl and lower than that for NSAID salts, being in agreement with the hydrophilic–hydrophobic characteristics of each API salt as discussed above. Differences between the API-IL uptake could

be assigned to the different API and API-IL molecular weights and chemical and physical structures. Among the studied API-ILs, the highest and lowest membrane uptakes were observed for [Lido][Diclo] and [Lido][Ibu], respectively. The membrane uptake was compared between each noncharged drug and API-ILs. It is shown that less hydrophobic drugs (higher water solubility) stay for a shorter time in the PVDF membrane pores.

The same uptake trend has been observed with the PVDF/HA membranes. The uptake of API-ILs was higher than those observed with lidocaine and lidocaine.HCl but lower than those obtained with the noncharged NSAIDs and NSAID salts. Generally, the drug uptake capacity of PVDF/HA is lower than that of PVDF.

**Table 4.** PVDF and PVDF/HA membrane uptake of API-ILs, APIs, and APIs salts.

| | | **PVDF (Uptake ± σ)%** | **PVDF/HA (Uptake ± σ)%** |
|---|---|---|---|
| API-ILs | [Lido][Ibu] | 15.8 ± 0.5 | 13.9 ± 0.3 |
| | [Lido][Nap] | 16.1 ± 0.3 | 14.2 ± 0.1 |
| | [Lido][Diclo] | 16.3 ± 0.3 | 14.4 ± 0.2 |
| API sodium salts | Lidocaine.HCl | 3.7 ± 0.1 | 3.2 ± 0.4 |
| | Ibuprofen.Na | 19.1 ± 0.2 | 17.2 ± 0.3 |
| | Naproxen.Na | 19.7 ± 0.3 | 17.7 ± 0.4 |
| | Diclofenac.Na | 20.3 ± 0.2 | 18.5 ± 0.5 |
| Noncharged APIs | Lidocaine | 5.7 ± 0.5 | 5.1 ± 0.6 |
| | Ibuprofen | 20.6 ± 0.4 | 18.7 ± 0.5 |
| | Naproxen | 21.2 ± 0.5 | 19.1 ± 0.4 |
| | Diclofenac | 21.7 ± 0.6 | 19.5 ± 0.3 |

The release of API-ILs and their corresponding drugs from PVDF and PVDF/HA membranes was determined through HPLC by the quantification of both ions, additionally proving that both ions are released in a close equimolar amount. Detailed data are given in the Supporting

Information (Table S4). The cumulative release profile of the prepared API-ILs and original noncharged drugs from the PVDF and PVDF/HA membranes are shown in Figure 6.

Studies from both PVDF and PVDF/HA membranes show a low cumulative drug release for the noncharged APIs because of the low solubility and high hydrophobic behavior of NSAIDs, as expected. Lidocaine and diclofenac present the highest and lowest amounts of release, respectively. Lidocaine is more soluble in water, but its hydrophilic behavior not only prevents the membrane from absorbing this API but also leads to its burst release. The fast release of lidocaine from the PVDF and PVDF/HA membrane pores occurred after 2 and 6 h, respectively. Overall, the release of NSAIDs follows their corresponding solubility: ibuprofen > naproxen > diclofenac. In this case, strong hydrophobic interactions between the PVDF membrane and NSAIDs prevent the complete release of drugs from the membrane pores. The same release trend is observed for the API-ILs: [Lido][Ibu] > [Lido][Nap] > [Lido][Diclo]. In contrast to the noncharged NSAIDs, dual-biological function API-ILs, in combination with a more water-soluble drug such as lidocaine and less water-soluble NSAIDs, show a higher cumulative release. Remarkably, API-ILs allow an increase in the cumulative release from PVDF and PVDF/HA membranes up to 85-97% and 80-90%, achieved at 72 and 120 h, respectively. The highest and lowest releases of API-ILs correspond to [Lido][Ibu] and [Lido][Diclo], respectively. The lower molecular weight and higher water solubility of [Lido][Ibu] could be considered as the main reason for the higher release observed with this API-IL. The higher release of lidocaine over [Lido][Diclo] is due to the more hydrophilic nature and higher water solubility of the first. Accordingly, lidocaine does not show a controlled release profile.

The release trend from the PVDF membranes is similar to the release trend from the PVDF/HA membranes, where API-ILs and NSAIDs have the highest and lowest releases, respectively. The

overall cumulative release in PVDF membranes is higher and faster than those in PVDF/HA membranes, which could be attributed the restrictive behavior of the HA layer. HA acts as a mass transfer-resistant layer, covering the PVDF membrane surface, while conditioning the exodus of APIs and API-ILs. However, the difference is less significant for the NSAID release because of the stronger hydrophobic interactions occurring between PVDF and NSAIDs.

Overall, not only there was a higher release of API-ILs than of APIs from the PVDF and PVDF/HA membranes, but also these compounds will lead to an improved bioavailability because of their higher water solubility and dual analgesic and anti-inflammatory properties [85]. A similar behavior was reported in the case of Lidocainium-Docusate [86].

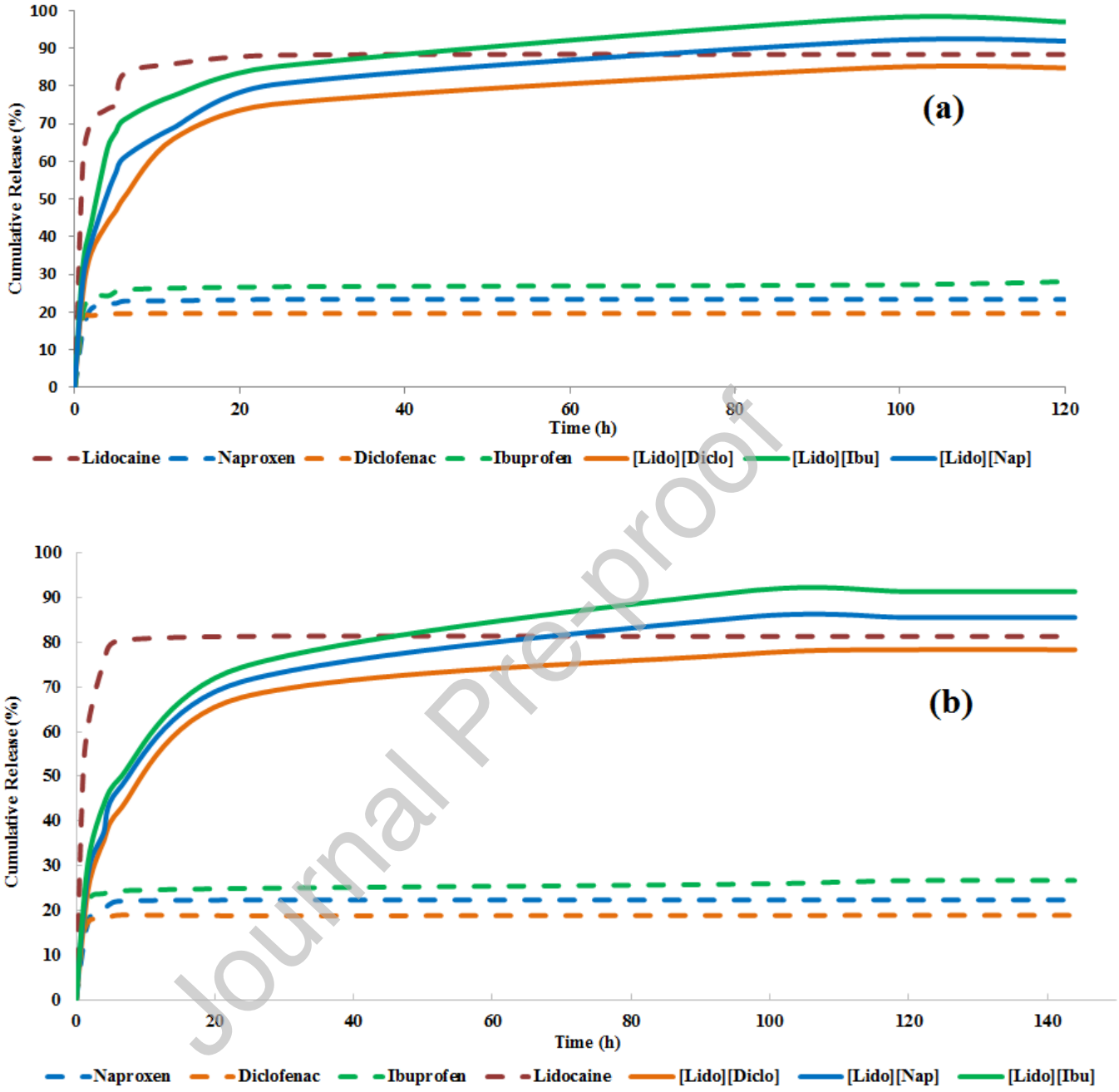




**Figure 6.** Cumulative release of APIs and API-ILs at 37 °C from (a) PVDF and (b) PVDF/HA membranes.

Transdermal delivery and skin permeation of API-ILs and APIs were also investigated. The cumulative release profile within time is shown in Figure 7. When compared with the previous

assays, the overall cumulative release decreases, whereas the required time for reaching a constant cumulative release increases. This behavior is due to additional mass transfer effects provided by the skin, limiting the permeation of APIs and API-ILs. However, the permeation of API-ILs into the skin is higher than that observed with NSAIDs. Furthermore, as observed before, lidocaine has a burst release.

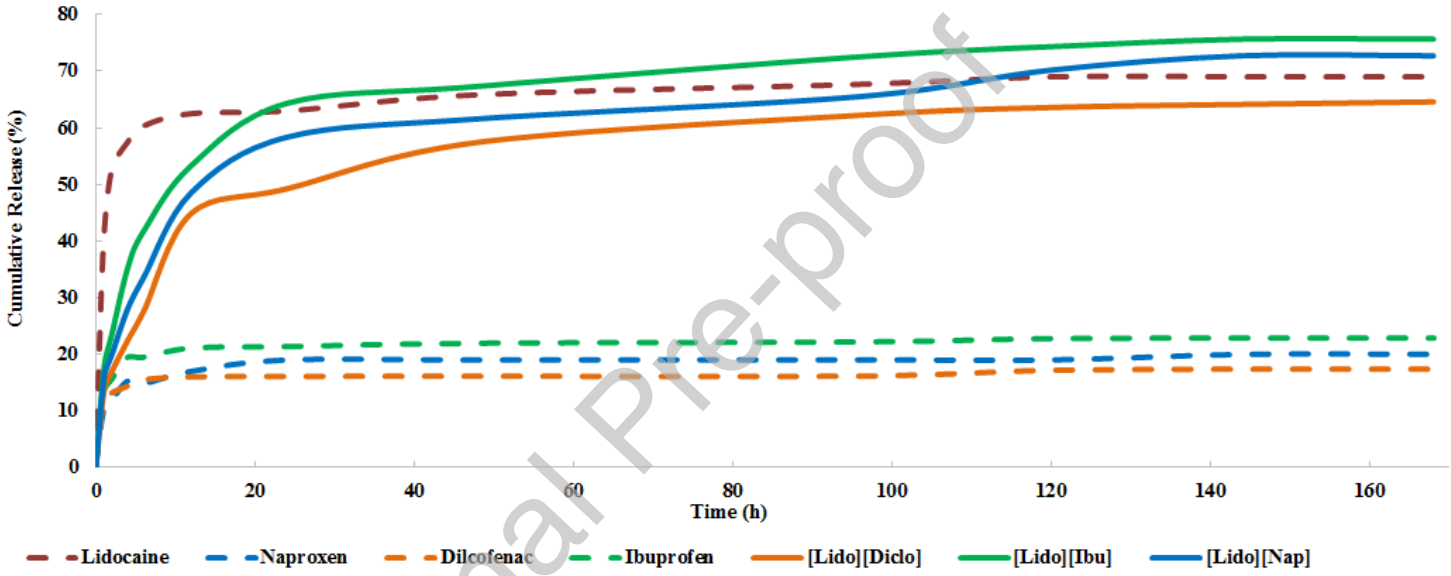


**Figure 7.** Cumulative release profile in the transdermal delivery of APIs and API-ILs from PVDF/HA membranes at 37°C.

### 3.3 Biological Assays

#### 3.3.1 Cell adhesion assays

Representative SEM images of cell adhesion on the PVDF and PVDF/HA membranes (loaded and unloaded with API-ILs) are shown in Figure 8. For all API-ILs, the density of adhered fibroblasts on the membrane increases after grafting HA on the PVDF surface, being in agreement with the reported beneficial effects of HA on fibroblast migration and proliferation

[21]. Furthermore, the expanded shapes of fibroblast cells confirm their viability and tendency to interact with other cells.

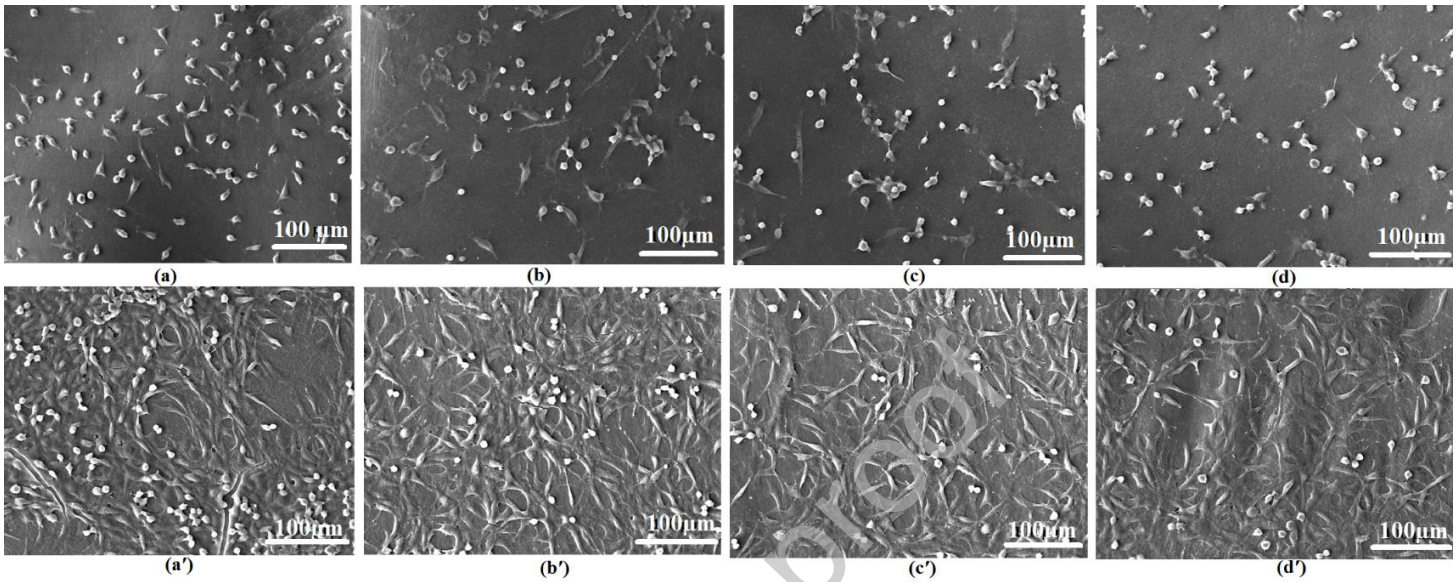


**Figure 8.** Cell adhesion to membranes of (a) PVDF, (b) PVDF loaded with [Lido][Ibu], (c) PVDF loaded with [Lido][Nap], d) PVDF loaded with [Lido][Diclo], (a′) PVDF/HA, (b′) PVDF/HA loaded with [Lido][Ibu], (c′) PVDF/HA loaded with [Lido][Nap], and (d′) PVDF/HA loaded with [Lido][Diclo]. The scale bars correspond to 100 µm.

### 3.3.2 Cell viability assays

Cell viability assays were performed using Raw 264.7 macrophages and fibroblasts for APIs, API-ILs, and PVDF/HA membranes loaded with API-ILs. The results of macrophage and fibroblast viabilities are depicted in Figures 9 and 10, respectively.

Among all the original APIs tested, lidocaine showed the lowest negative effect on cells, maintaining their viability at 100% for all the concentrations tested in both assays. On the other hand, the remaining noncharged APIs decrease the cell viability in the following order: diclofenac > ibuprofen > naproxen. The cytotoxicity displayed by these APIs is in line with that reported in the literature [87].

The results of the resazurin assay demonstrate that the API-IL cytotoxicity profile follows the same trend as that of the respective APIs. [Lido][Ibu] presents a similar dose–response curve, while both [Lido][Diclo] and [Lido][Nap] present a slight toxicity increase at higher concentrations. Nevertheless, it should be remarked that it is the improved solubility of API-ILs that will reduce the amount of drug needed to obtain the desired anti-inflammatory effect on cells. Furthermore, the PVDF/HA membranes display a similar trend in the cytotoxicity profile as that displayed by API-ILs. The results also demonstrate that the investigated membranes are nontoxic. Overall, this set of results is of relevance, as they define the amount of each API-IL that could be loaded into the prepared PVDF/HA membranes to be safely used.

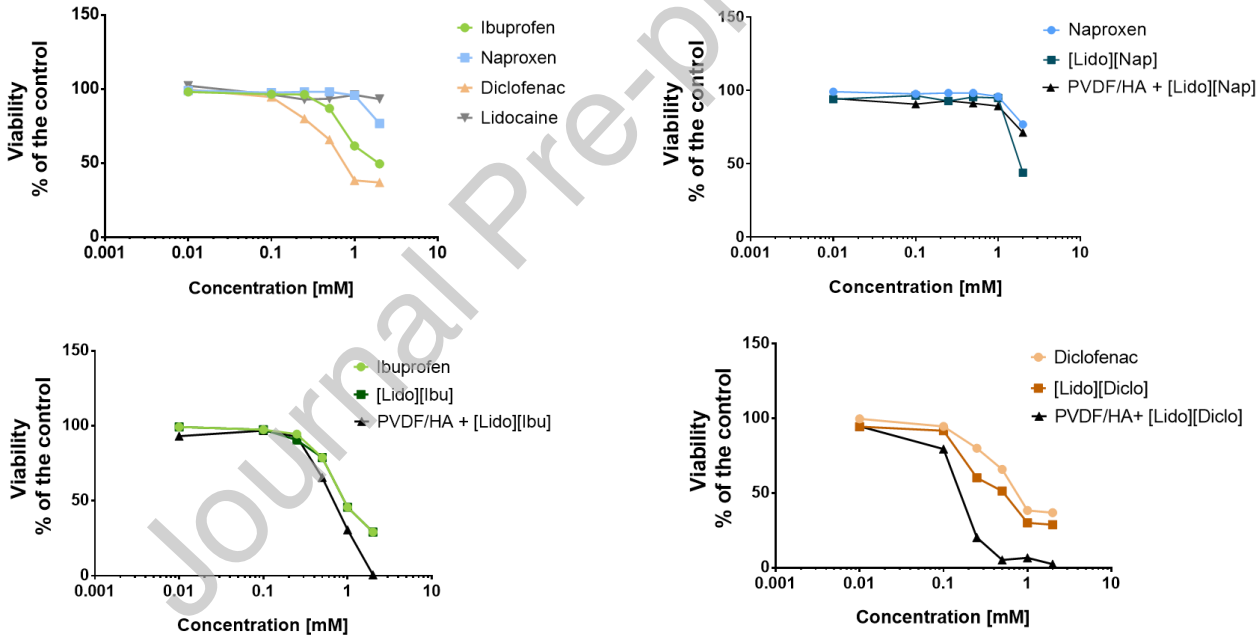


**Figure 9.** Effects of the noncharged APIs, API-ILs, and PVDF/HA membranes loaded with API-ILs on macrophage cell viability.

The toxicity of APIs, API-ILs, and PVDF and PVDF/HA membranes loaded with API-ILs for fibroblasts was additionally investigated by the MTT assay. API-ILs lead to a decrease in the cell

viability by increasing their concentration and for which the highest toxicity was observed with [Lido][Diclo]. However, all API-ILs demonstrated high cell viability up to 1 mM. Furthermore, the fibroblast viability enhances in PVDF/HA membranes loaded with API-ILs, while the cell viability decreases in PVDF membranes loaded with API-ILs. The biocompatible behavior of the HA layer, which is in direct contact with the fibroblast cells, could explain the observed cell viability enhancement, being also in agreement with the cell adhesion results. On the other hand, HA restricts the release of API-ILs, and as such, the negative effect of API-ILs on the cell viability decreases after HA grafting on the PVDF surface.

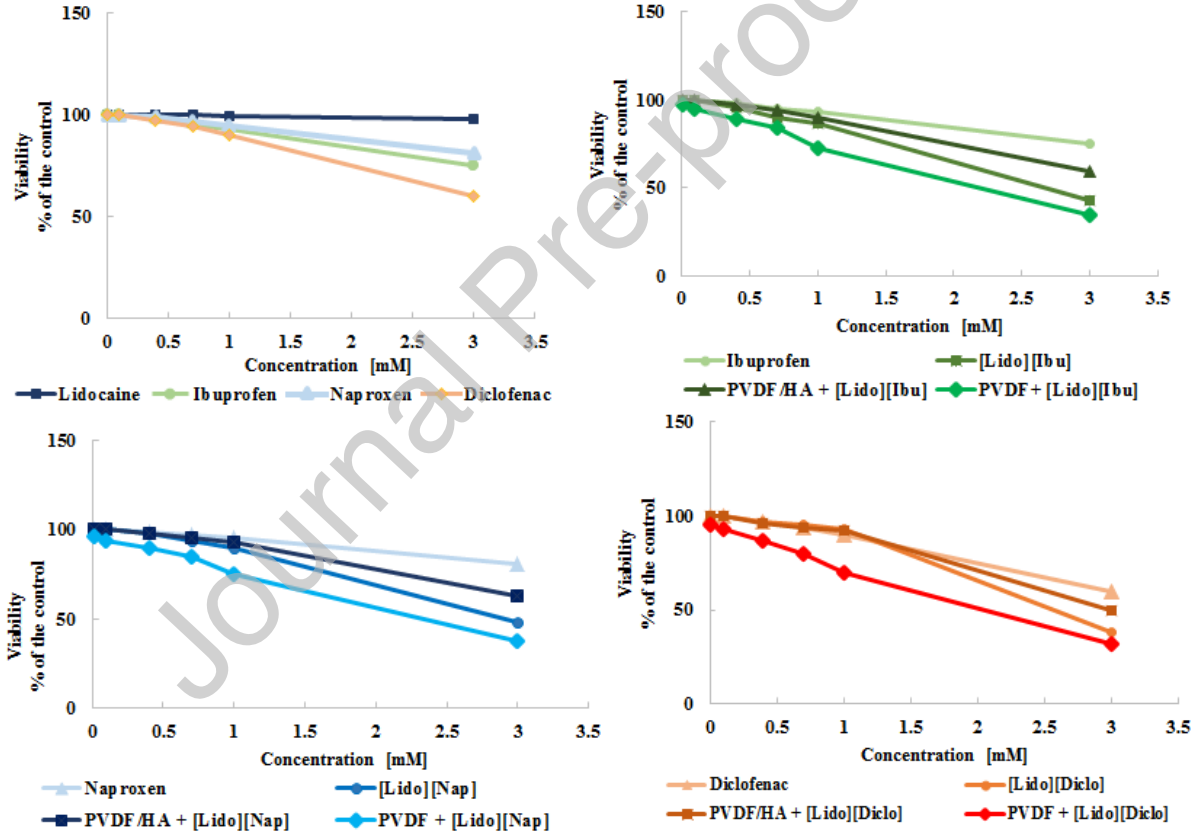


**Figure 10**. Effects of the noncharged APIs, API-ILs, and PVDF/HA and PVDF membranes loaded with API-ILs on fibroblast cell viability.

### 3.3.3 Anti-inflammatory assays

The anti-inflammatory activity of PVDF/HA membranes loaded with API-ILs was investigated in macrophages (Raw 264.7) activated with *E. coli* lipopolysaccharide (LPS) and compared with the corresponding noncharged NSAIDs. The impact of the membranes on the NO production was first evaluated (Figure 11) and compared with the respective API. The results demonstrate that the unloaded membranes do not provoke an inflammatory response, as the NO production values are comparable to the control, indicating that the material is immunologically safe. Furthermore, both the precursor APIs and the PVDF/HA membranes loaded with API-ILs have a modest but still significant effect in decreasing the NO production. These results are expected, as the main mechanism of action of the used NSAID drugs does not rely on NO synthesis inhibition but instead on the inhibition of the cyclooxygenase-2 (COX-2) enzyme, thus mitigating the production of pro-inflammatory prostaglandins [88].

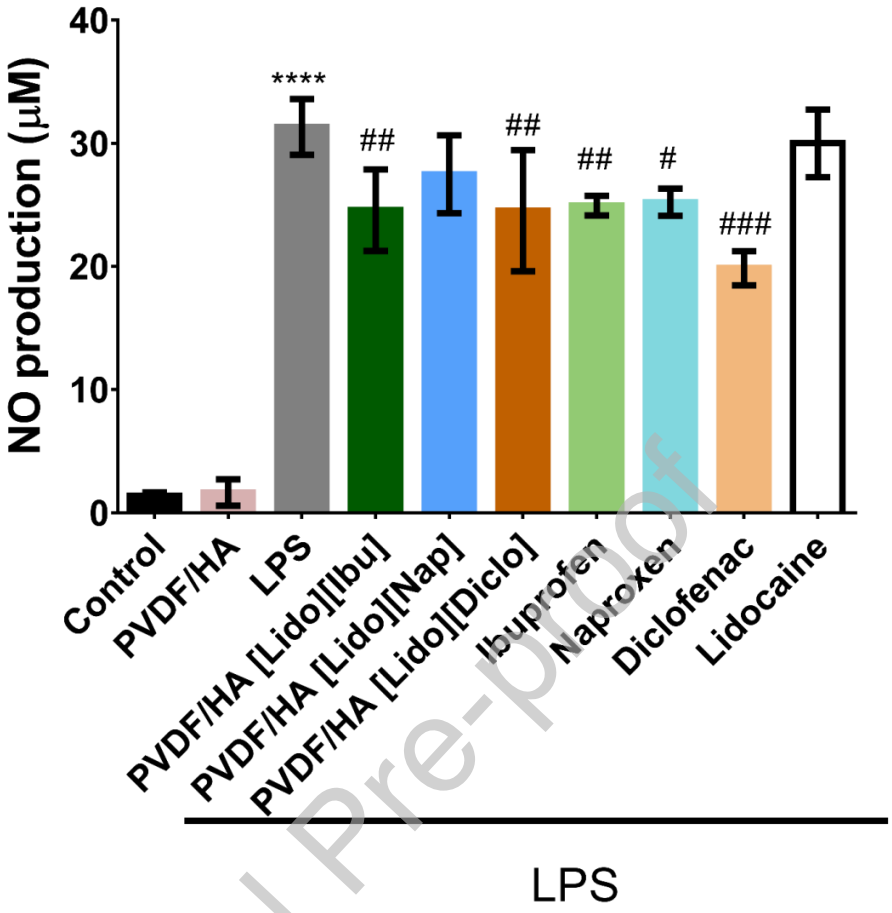


**Figure 11.** Effect of the noncharged APIs and PVDF/HA membranes loaded with the API-ILs on nitric oxide production of LPS-activated macrophages. Data are presented as the amount of NO production and represented as the average ± standard deviation from at least 3 independent biological experiments. (****p<0.0001; control vs. LPS; $^{\#}$p<0.05; $^{\#\#}$p<0.01, $^{\#\#\#}$p<0.001: PVDF/HA membranes vs. LPS).

On the basis of the previous information, the inhibition of LPS-induced prostaglandin E2 (PGE2) production caused by drugs was also tested, whose results are depicted in Figure 12. PVDF/HA membranes do not provoke significant macrophage activation as can be addressed by the modest PGE2 production. However, the PVDF/HA membranes loaded with API-ILs have the capacity to inhibit COX2 and thus decrease the PGE2 release in the same magnitude as that of the precursor

noncharged APIs. The decrease in PGE2 production is highly significant, which is consistent with the reported anti-inflammatory effects in the literature for these APIs [89,90]. On the other hand, lidocaine does not display any anti-inflammatory effect as expected because it is an analgesic drug. These results also indirectly support the good and predictable release profile of API-ILs from the PVDF/HA membranes.

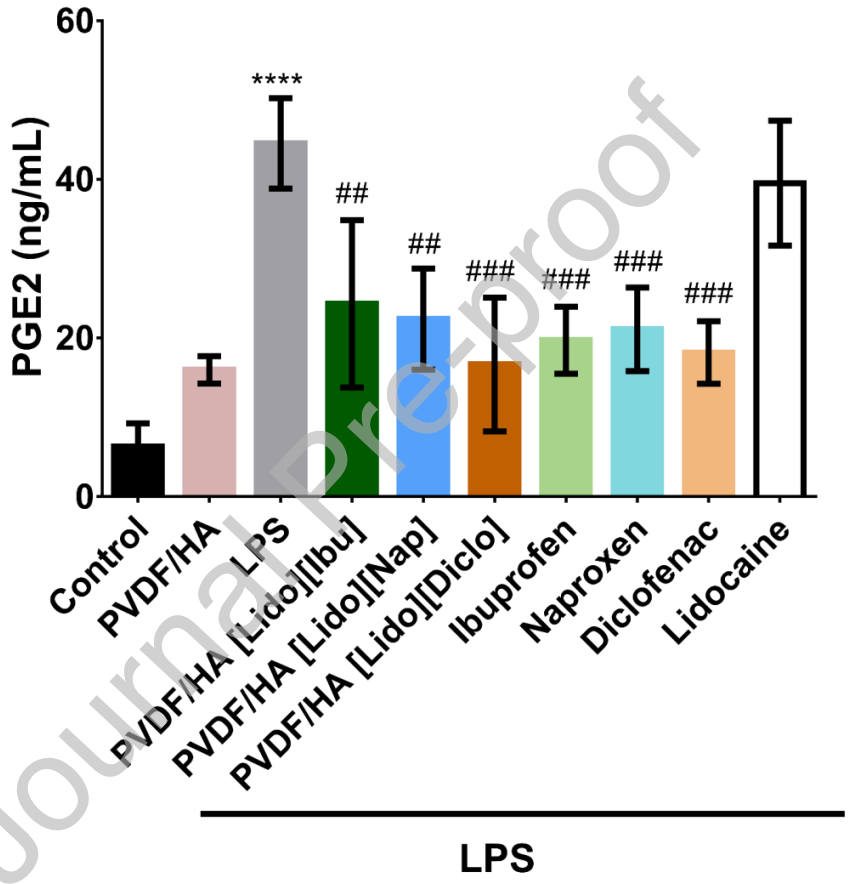


**Figure 12.** Effect of noncharged APIs and PVDF/HA loaded with API-ILs in the LPS-induced PGE2 production. Data are presented as the amount of PGE2 production and represented as the average ± standard deviation from at least 3 independent biological experiments. (****$p<0.0001$; control vs. LPS; $^{\#}p<0.05$; $^{\#\#}p<0.01$, $^{\#\#\#}p<0.001$: PVDF/HA membranes vs. LPS).

### 3.3.4 Wound healing assays

The wound healing process highly depends on the fibroblast proliferation and migration from neighboring connective tissues to the injured area. Therefore, the impact of conditioned media from PVDF or PVDF/HA membranes loaded with API-ILs on the spreading and migration behavior of these cells across a wound area was finally evaluated *in vitro* (Figure 13). All assays were performed in a medium with 2% FBS, except when 10% FBS is used as the positive control. Cytochalasin D (CITO D) was used as a negative control, blocking actin polymerization and inducing cell cycle arrest. As expected, at high concentrations of FBS, the increased cell proliferation rate and the almost complete occlusion of the wound were observed. Moreover, the PVDF/HA membranes without API-ILs (unloaded membranes) do not interfere with the fibroblast proliferation/migration, as the dimension of the gap after 16 h is similar to the respective control (2% FBS).

The PVDF/HA membranes loaded with [Lido][Ibu] and [Lido][Nap] do not negatively impact the fibroblast proliferation, while [Lido][Diclo] causes a slight inhibition in cell proliferation/migration. In the literature, there are some conflicting reports on the impact of NSAIDs on fibroblast proliferation, including the negative effects that are usually related to the concentrations used [91, 92]. These antiproliferative properties over fibroblasts were shown to rely on COX-2 inhibition and consequent decreased levels of prostaglandin E2 [93]. NSAIDs may additionally impair wound healing by decreasing the activity of the enzyme prolidase, which results in a decrease in collagen biosynthesis by fibroblasts [94, 95].

HA has been shown to play multiple beneficial effects on wound healing processes, namely, by enhancing angiogenesis and by promoting fibroblast proliferation and capacity to synthesize collagen and enzymes linked to the extracellular matrix remodeling [96]. Accordingly, HA has been extensively used as a central component in scaffolds and dressing membranes, with an aim

to accelerate skin regeneration [97–99]. To address whether the incorporation of HA in the membranes contributes to mitigate some of the potential negative effects of NSAIDs on fibroblast proliferation, parallel experiments were performed with simple PVDF structures loaded with API-ILs. As shown in Figure 13, the capacity of fibroblasts to colonize the gap is lower in PVDF membranes loaded with API-ILs than with their respective PVDF/HA membranes loaded with API-ILs. Results from cytotoxicity/proliferation assays also revealed a similar tendency in which the presence of HA exerts a protective effect (Figure S5 in the Supplementary Information). Therefore, in the membranes studied here, HA minimizes potential antiproliferative effects attributable to NSAIDs, allowing the simultaneous delivery of anti-inflammatory and analgesic drugs to the injured area without compromising skin regeneration.

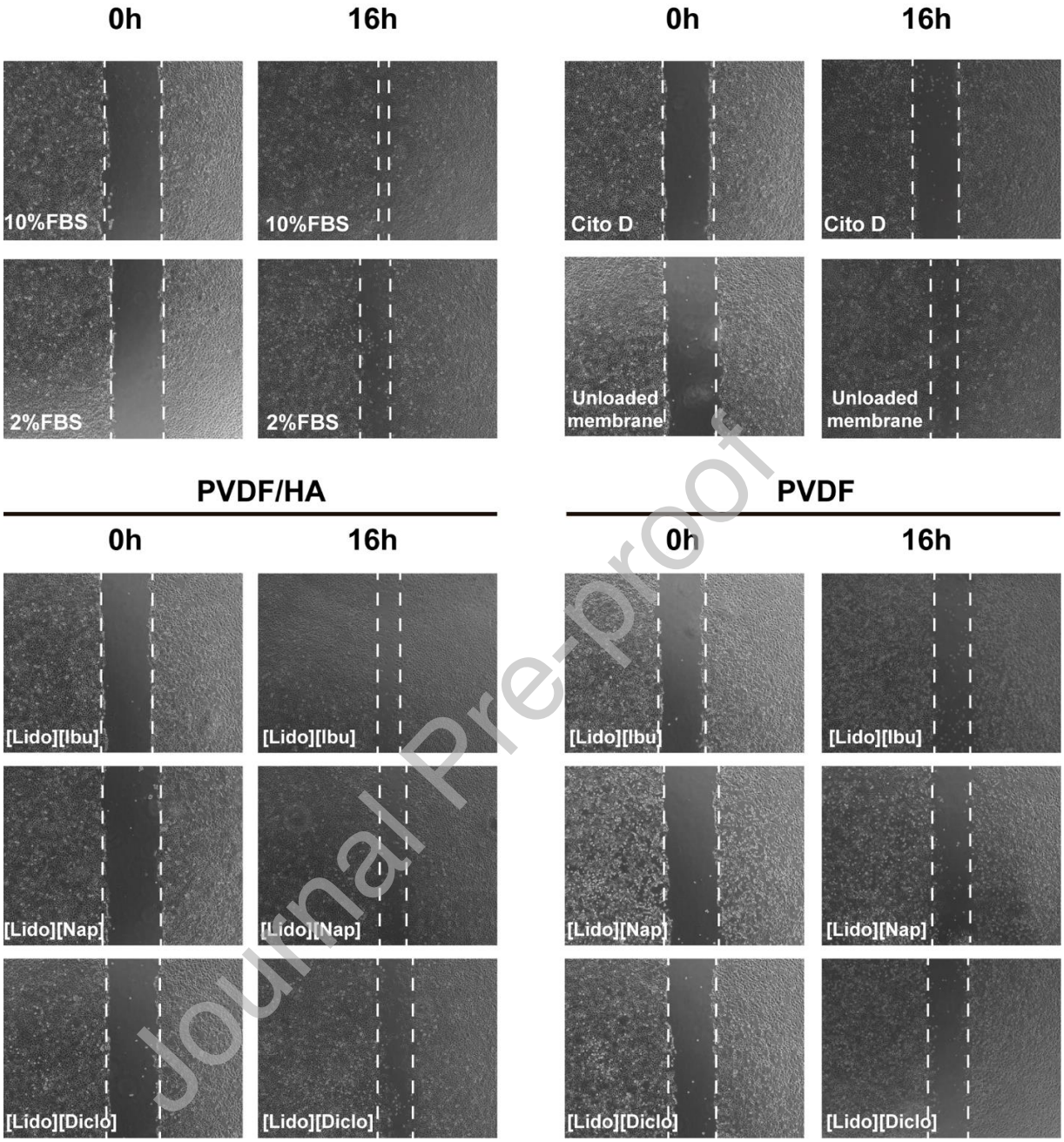


**Figure 13.** Impact of PVDF and PVDF/HA membranes loaded with API-ILs in fibroblast proliferation/migration. Scratch wound assays were performed with 3T3 fibroblasts treated with conditioned media from PVDF-API-IL and PVDF/HA-API-IL membranes. Images were captured at 0 h and 16 h time points using an Evos M5000 Cell imaging System at 4x magnification.

## 4. Conclusions

Bilayer wound dressings composed of a hydrophobic PVDF membrane and a hydrophilic HA layer were first prepared to act as a drug reservoir and to have biocompatible characteristics on contact with skin, respectively, containing dual-biological function ILs and then characterized. To this end, API-ILs, comprising both analgesic and anti-inflammatory properties, were synthesized and characterized by combining a cation derived from lidocaine and anions derived from hydrophobic NSAIDs. All prepared API-ILs are liquid at room temperature and display high degradation temperatures. All the determined properties were compared with those of the original drugs. By converting the original drugs into dual-function API-ILs, there is an increase in their water solubility up to 470-fold, without significantly affecting their cytotoxic profile. Both the IL cation and anion were quantified, indicating that they solubilize in water in a 1:1 molar ratio.

The prepared bilayer wound dressing was characterized in terms of mechanical properties, membrane uptake and drug release, and transdermal delivery behavior. The PVDF membrane layer provided the required mechanical stability of bilayer wound dressing, while HA grafting on the PVDF membrane surface enhanced fibroblast cell proliferation, migration, and adhesion. Furthermore, the PVDF/HA membranes do not cause activation of macrophages, indicating that they are immunologically safe and biocompatible.

The release of API-ILs is higher than that of the original NSAID drugs in PVDF and PVDF/HA membranes, contributing to desirable analgesic and anti-inflammatory characteristics for wound healing purposes. Fibroblast cell adhesion and cell viability are improved with the grafting of HA onto the PVDF membrane surface. Finally, it was shown that membranes loaded with the API-ILs display a similar anti-inflammatory effect on LPS-activated macrophages as that of the

precursor APIs and that the unloaded and loaded membranes do not negatively affect fibroblast proliferation and migration in in vitro wound healing assays, thus presenting a safety profile to be used as effective transdermal drug delivery systems.

**Conflict of interest**

The authors declare no competing financial interest.

**Acknowledgments**

This work was developed within the scope of the project CICECO-Aveiro Institute of Materials, FCT Ref. UID/CTM/50011/2019, financed by national funds through the FCT/MCTES. The authors acknowledge the financial support from the European Union Framework Programme for Research and Innovation HORIZON 2020, under the TEAMING Grant agreement No. 739572 – The Discoveries CTR. M.G. Freire acknowledges the European Research Council under the European Union's Seventh Framework Programme (FP7/2007-2013)/ERC grant agreement no. 337753.

**References**

[1] U.D.S. Sekhon and A.S. Gupta, Platelets and Platelet-Inspired Biomaterials Technologies in Wound Healing Applications. ACS Biomater. Sci. Eng. 4 (2018) 1176–1192.

[2] S. Guo and L.A. DiPietro, Factors Affecting Wound Healing. J Dent Res 89 (2010) 219-229.

[3] K. Anderson and R.L. Hamm, Factors that Impair Wound Healing. J Am Coll Clin Wound Spec 4 (2014) 84-91.

[4] A. Ghaee, M. Karimi, M. Lotfi, B. Sadatnia and V. Hosseinpour, Preparation of hydrophilic polycaprolactone/modified ZIF-8 nanofibers as a wound dressing using hydrophilic surface modifying macromolecules, Mater. Sci. Eng.,C. 103 (2019) 109767.

[5] Y. Xi, H. Dong, K. Sun, H. Liu, R. Liu, Y. Qin, Z. Hu, Y. Zhao, F. Nie, and S. Wang, Scab-Inspired Cytophilic Membrane of Anisotropic Nanofibers for Rapid Wound Healing, ACS Appl. Mater. Interfaces 5 (2013) 4821–4826.

[6] S.S. Silva, E.G. Popa, M.E. Gomes, M. Cerqueira, A.P. Marques, S.G. Caridade, P. Teixeira, C. Sousa, J.F. Mano and R.L. Reis, An investigation of the potential application of chitosan/aloebased membranes for regenerative medicine. Acta Biomater. 9 (2013) 6790–6797.

[7] Y. Li, Y. Han, X. Wang, J. Peng, Y. Xu, and J. Chang, Multifunctional Hydrogels Prepared by Dual Ion Cross-Linking for Chronic Wound Healing, ACS Appl. Mater. Interfaces 9 (2017) 16054–16062.

[8] V. Coger, N. Million, P. Wilke, A. Pich, P.M. Vogt, and K. Reimers, Laser-generated bioactive hydrogels as ion-release systems for burn wound therapy, in Optically Induced Nanostructures: Biomedical and Technical Applications, Chapter 3, 199-216, 2015.

[9] P. Rana, G. Ganarajan, and P. Kothiyal, Review on transdermal drug delivery system, World J. Pharm. Sci. 5 (2016) 556–567.

[10] D.H. Kim, J.H. Park, S.J. Seo, J.S. Park, S. Jung, Y.S. Kang, J.H. Choi, M.S. Kang, Development of thin anion-exchange pore-filled membranes for high diffusion dialysis performance, J. Memb. Sci. 447 (2013) 80–86.

[11] C.K. Sahoo, P.K. Nayak, and T.K. Sahoo, A Review of Transdermal drug delivery system", J. der Pharm. Forsch. 2 (2013) 32–56.

[12] S. Tohidi, A. Ghaee, and J. Barzin, Preparation and characterization of poly(lactic-co-glycolic acid)/chitosan electrospun membrane containing amoxicillin-loaded halloysite nanoclay, Polym. Adv. Technol. 27 (2016) 1020–1028.

[13] A. Mashak, A. Ghaee and F. Ravari, Effect of poly(N-vinypyrolidone) on the non-isothermal crytalization kinetics and viscoelastic properties of PVDF films, Braz. J. Chem. Eng. 33 (2016) 945-956.

[14] Y. Nakagawa, S. Nakasako, S. Ohta, and T. Ito, A biocompatible calcium salt of hyaluronic acid grafted with polyacrylic acid", Carbohydr. Polym. 117 (2015) 43–53.

[15] W. Gao, T. Lin, T. Li, M. Yu, X. Hu, and D. Duan, Sodium alginate/heparin composites on PVC surfaces inhibit the thrombosis and platelet adhesion: Applications in cardiac surgery, Int. J. Clin. Exp. Med. 6 (2013) 259–268.

[16] S. Van Vlierberghe, E. Vanderleyden, V. Boterberg, and P. Dubruel, Gelatin functionalization of biomaterial surfaces: Strategies for immobilization and visualization, Polymers 3 (2011) 114–130.

[17] Y. L. Cui, A. D. Qi,W. G. Liu, X. H. Wang, H. Wang, D. M. Ma, and K. D. Yao, Biomimetic surface modification of poly(L-lactic acid) with chitosan and its effects on articular chondrocytes in vitro, Biomaterials 24 (2003) 3859–3868.

[18] H.D. Park, J.W. Bae, and K.D. Park, Surface Modification of Polyurethane Using Sulfonated PEG Grafted Polyrotaxane for Improved Biocompatibility, Macromol. Res. 14 (2006) 73–80.

[19] S.K. Seidlits, C.T. Drinnan, R.R. Petersen, J.B. Shear, L.J. Suggs, and C.E. Schmidt, Fibronectin-hyaluronic acid composite hydrogels for three-dimensional endothelial cell culture, Acta Biomater. 7 (2011) 2401-2409.

[20] F. Dosio, S. Arpicco, B. Stella, and E. Fattal, Hyaluronic acid for anticancer drug and nucleic acid delivery, Adv. Drug Deliv. Rev. 97 (2016) 204–236.

[21] R. M. A. Domingues, M. Silva, P. Gershovich, S. Betta, P. Babo, S. G. Caridade, J. F. Mano, A. Motta, R. L. Reis, and M. E. Gomes, Development of Injectable Hyaluronic Acid/Cellulose Nanocrystals Bionanocomposite Hydrogels for Tissue Engineering Applications, Bioconjug. Chem. 26 (2015) 1571–1581.

[22] S. Thönes, S. Rother, T. Wippold, J. Blaszkiewicz, K. Balamurugan, S. Moeller, G. Ruiz-Gómez, M. Schnabelrauch, D. Scharnweber, A. Saalbach, J. Rademann, M.T. Pisabarro, V. Hintze and U. Anderegg, Hyaluronan/collagen hydrogels containing sulfated hyaluronan improve wound healing by sustained release of heparin-binding EGF-like growth factor, Acta Biomater. 86 (2019) 135-147.

[23] B.E. Hosseinzadeh, M. Pedram, A. Hatamian, S. Salahshour, M. Rasti, Z.B. Mokhtar-Hosseini and M. Mir- Derikvand, In vivo Evaluation of Gelatin/Hyaluronic Acid Nanofiber as Burn-wound Healing and Its Comparison with ChitoHeal Gel, Fibers and Polymers. 17 (2016) 820-826.

[24] A. Mohandas, B.S. Anisha, K.P. Chennazhi, and R. Jayakumar, Chitosan-hyaluronic acid/VEGF loaded fibrin nanoparticles composite sponges for enhancing angiogenesis in wounds, Coll. Surf. B 127 (2015) 105–113.

[25] Y.K. Lin, Y. Matsumoto, Y. Kuroyanagi, and S. Kagawa, A Bilayer Hyaluronic Acid Wound Dressing to Promote Wound Healing in Diabetic Ulcer, J. Bioact. Compat. Polym. 24 (2009) 424–443.

[26] Y. Matsumoto, K. Arai, H. Momose, and Y. Kuroyanagi, Development of a Wound

Dressing Composed of a Hyaluronic Acid Sponge Containing Arginine, J. Biomater. Sci. Polym. 20 (2009) 993–1004.

[27] H. Roehrs, J. G. D. Stocco, F. Pott , G. Blanc, K. Crozeta , M. J. Meier, F. A. L. Dias., Dressings and topical agents containing hyaluronic acid for chronic wound healing, Cochrane Database Syst. Rev. 2016 (2016) 1-16.

[28] H. E. Thu, M. H. Zulfakar, and S. F. Ng, Alginate based bilayer hydrocolloid films as potential slow-release modern wound dressing, Int. J. Pharm. 434 (2012) 375–383.

[29] A. T. M. Serajuddin, Salt formation to improve drug solubility, Adv. Drug Deliv. Rev. 59 (2007) 603–616.

[30] P. C. A. G. Pinto and M. L. M. F. S. Saravia, Ionic Liquids: A Pharmaceutical perspective, Pinto Ionica, vol. 13, 2013, p. 6147.

[31] K. Bica, H. Rodríguez, G. Gurau, C. O. Andreea, A. Riisager, R. Fehrmann, R. D. Rogers, Pharmaceutically active ionic liquids with solids handling, enhanced thermal stability, and fast release, Chem. Commun. 48 (2012) 5422-5424.

[32] H. D. Williams, Y. Sahbaz, L. Ford, T. H. Nguyen, P. J. Scammells, and C. J. H. Porter, Ionic liquids provide unique opportunities for oral drug delivery: structure optimization and in vivo evidence of utility, Chem. Commun. 50 (2014) 1688–1690.

[33] H. Koga, M. Nogi, and A. Isogai, Ionic Liquid Mediated Dispersion and Support of Functional Molecules on Cellulose Fibers for Stimuli-Responsive Chromic Paper Devices, ACS Appl. Mater. Interfaces 9 (2017) 40914–40920.

[34] Z. Zheng, Q. Xu, J. Guo, J. Qin, H. Mao, B. Wang, F. Yan, "tructure-Antibacterial Activity Relationships of Imidazolium-Type Ionic Liquid Monomers, Poly(ionic liquids) and Poly(ionic liquid) Membranes: Effect of Alkyl Chain Length and Cations, ACS Appl. Mater. Interfaces 8 (2016) 12684–12692.

[35] R. Ferraz, V. Teixeira, D. Rodrigues, R. Fernandes, C. Prudencio, J. P. Noronha, Z. Petrovski, L. Branco, Antibacterial activity of Ionic Liquids based on ampicillin against resistant bacteria, RSC Adv. 4 (2014) 4301–4307.

[36] R. Ferraz, L. C. Branco, C. Prudêncio, J. P. Noronha, and Ž. Petrovski, Ionic liquids as active pharmaceutical ingredients, Chem. Med. Chem. 6 (2011) 975–985.

[37] H. Mizuuchi, V. Jaitely, S. Murdan, and A. T. Florence, Room temperature ionic liquids and their mixtures: Potential pharmaceutical solvents, Eur. J. Pharm. Sci. 33 (2008) 326–

331.

[38] K. S. Egorova, E.G. Gordeev, and V. P. Ananikov, Biological Activity of Ionic Liquids and Their Application in Pharmaceutics and Medicine, Chem. Rev. 117 (2017) 7132–7189.

[39] K. Bica, C. Rijksen, M. Nieuwenhuyzen, and R. D. Rogers, In search of pure liquid salt forms of aspirin: ionic liquid approaches with acetylsalicylic acid and salicylic acid, Phys. Chem. Chem. Phys. 12 (2010) 1648–1648.

[40] H. J. Park and M. R. Prausnitz, Lidocaine-ibuprofen ionic liquid for dermal anesthesia, AIChE J. 61 (2015) 2732-2738.

[41] E. Sucman, J. Vavrinova, O. Synek and O. Sedlarik, Ion selective electrode methodfor the determination of sodium chloride in akawi cheeseand in brine, ACTA VET. BRNO 56 (1987) 151- 155.

[42] S. R. Dhaneshwar and V. K. Bhusari, Validated HPLC Method for Simultaneous Quantitation of Diclofenac Sodium and Misoprostol in Bulk Drug and Formulation, Der Chem. Sin. 1 (2010) 110–118.

[43] S. Ghalei, J. Nourmohammadi, A. Solouk, and H. Mirzadeh, Enhanced cellular response elicited by addition of amniotic fluid to alginate hydrogel-electrospun silk fibroin fibers for potential wound dressing application, Colloids Surf. B. 17 (2018) 82–89.

[44] A. Ghaee, B. Sadatnia, M. Khosravi, Z. Mansourpour, and A. Ghadimi, Preparation and characterization of modified PVDF membrane induced by argon plasma with enhanced antifouling property, Desalin. Water Treat. 64 (2017) 72-80.

[45] X. Yang, X. Wang, F. Yu, L. Ma, X. Pan, G. Luo, S. Lin, X. Mo, C. He, H. Wang, Hyaluronic acid/EDC/NHS-crosslinked green electrospun silk fibroin nanofibrous scaffolds for tissue engineering, RSC Adv. 6 (2016) 99720–99728.

[46] S.N. Park, J.C. Park, H.O. Kim, Min J. Song and H. Suh, Characterization of porous collagen/hyaluronic acid scaffold modified by 1-ethyl-3-(3-dimethylaminopropyl)carbodiimide cross-linking, Biomaterials 23 (2002) 1205-1212.

[47] D.V. Bax, N. Davidenko, D. Gullberg, S.W. Hamaia, R.W. Farndale, S.M. Best and R.E. Cameron, Fundamental insight into the effect of carbodiimide crosslinking on cellular recognition of collagen-based scaffolds, Acta Biomaterialia 49 (2017) 218-234.

[48] N. Davidenko, J.J. Campbell, E.S. Thian, C.J. Watson and R.E. Cameron, Collagen–

hyaluronic acid scaffolds for adipose tissue engineering, Acta Biomaterialia 6 (2010) 3957-3968.

[49] H. Shi, L. Xue, A. Gao, Y. Fu, Q. Zhou, and L. Zhu, Fouling-resistant and adhesion-resistant surface modification of dual layer PVDF hollow fiber membrane by dopamine and quaternary polyethyleneimine, J. Memb. Sci. 498 (2016) 39–47.

[50] S. M. Atyabi, F. Sharifi, S. Irani, M. Zandi, H. Mivehchi, and Z. Nagheh, Cell Attachment and Viability Study of PCL Nano-fiber Modified by Cold Atmospheric Plasma, Cell Biochem. Biophys. 74 (2016) 181–190.

[51] S. F. Ng, J. Rouse, D. Sanderson, and G. Eccleston, A Comparative study of transmembrane diffusion and permeation of ibuprofen across synthetic membranes using franz diffusion cells, Pharmaceutics 2 (2010) 209–223.

[52] J. Y. Fang, S.Y. Yu, P. C. Wu, Y.B. Huang and Y.H. Tsai, In vitro skin permeation of estradiol from various proniosome formulations, Int. J. Pharm. 215 (2001) 91–99.

[53] H.A.E. Benson and A.C. Watkinson, Transdermal and Topical Drug Delivery: Principles and Practice, 2012, chapt 5, In Vitro Skin Permeation Methodology, pp. 85-108.

[54] A.L.M. Ruela, A.G. Perissinato, M.E.S. Lino, P. S. Mudrik and G. R. Pereira, Evaluation of skin absorption of drugs from topical and transdermal formulations, Braz. J. Pharm 52 (2016) 527-544.

[55] A. Puri, S. A. Bhattaccharjee, W. Zhang, M. Clark, O. N. Singh, G. F. Doncel and A. K. Banga, Development of a Transdermal Delivery System for Tenofovir Alafenamide, a Prodrug of Tenofovir with Potent Antiviral Activity Against HIV and HBV, Pharmaceutics 11 (2019) 173.

[56] O. V. Zillich, U. Schweiggert-Weisz, K. Hasenkopf, P. Eisner and M. Kerscher, Release and in vitro skin permeation of polyphenols from cosmetic emulsions, INT J COSMETIC SCI 35 (2013) 491–501.

[57] J. O. Brien, I. Wilson, T. Orton, and Ë. Pognan, Investigation of the Alamar Blue (resazurin) fluorescent dye for the assessment of mammalian cell cytotoxicity, J. Biochem. 5426 (2000) 5421–5426.

[58] A. Abednejad, A, Ghaee, J. Nourmohammadi and A. Abouei mehrizi, Hyaluronic acid/ carboxylated Zeolitic Imidazolate Framework film with improved mechanical and antibacterial properties, Carbohyd Polym. 222 (2019) 115033.

[59] Z. Hadisi, J. Nourmohammadi and S.M. Nasiri, The antibacterial and anti-inflammatory investigation of Lawsonia Inermis-gelatin-starch nano-fibrous dressing in burn wound. Int J Biol Macromol, 107 (2018) 2008–2019.

[60] H. Wang, G. Gurau, J. Hamshina, O.A. Cojocaru, J. Janikowski, D.R. MacFarlane, J.H. Davis, and R. D. Rogers, Simultaneous membrane transport of two active pharmaceutical ingredients by charge assisted hydrogen bond complex formation, Chem. Sci. 5 (2014) 3449–3456.

[61] W. L. Hough, Functional Ionic Liquids for use in Pharmaceutical Applications, University of Alabama Libraries, 2010.

[62] Spectrum Chemical MGF Corp at http://spectrumchemical.com.

[63] Fischer Scientific at http://Fishersci.com.

[64] B. Tiţa, A. Fuliaş, G. Bandur, G. Rusu, and D. Tiţa, Rev. Roum. Chim. 55 (2010) 553-558.

[65] Tita et. al., Rev. Chim., 62 (2011) 216–221, 2011.

[66] W. M. Haynes, CRC Handbook of Chemistry and Physics, pp. 3-172, 2013.

[67] PubChem at https://pubchem.ncbi.nlm.nih.gov.

[68] M.R. Sovizi, Thermal behavior of drugs, J. Therm. Anal. Calorim. 102 (2010) 285–289.

[69] P. Tudja, M. Z. I. Khan, E. Mestrovic, M. Horvat, and P. Golja, Thermal Behaviour of Diclofenac Sodium: Decomposition and Melting Characteristics, Chem. Pharm. Bull 49 (2001) 1245–1250.

[70] M. J. O'Neil, The Merck Index- An Encyclopedia of Chemicals, Drugs, and Biologicals, Whitehouse Station, p. 522, 2006.

[71] J. Ranke, A. Othman, P. Fan, and A. Müller, Explaining ionic liquid water solubility in terms of cation and anion hydrophobicity, Int. J. Mol. Sci. 10 (2009) 1271–1289.

[72] M. Ishikawa and Y. Hashimoto, Improvement in aqueous solubility in small molecule drug discovery programs by Disruption of Molecular Planarity and Symmetry, J. Med. Chem. 54 (2011) 1539–1554.

[73] I. Ali , O. A. Bamaga, L. Gzara, M. Bassyouni, M. H. Abdel-Aziz, M. F. Soliman, E. Drioli, M. Albeirutty, Assessment of blend PVDF membranes, and the effect of polymer concentration and blend composition, Membranes (Basel)., vol. 8, no. 1, 2018.

[74] S. Karimi, A. Ghaee, and J. Barzin, Preparation and characterization of a piezoelectric

poly(vinylidene fluoride)/nanohydroxyapatite scaffold capable of naproxen delivery, Eur. Polym. J. 112 (2019) 442–451.

[75] A. Rahimpour, S. S. Madaeni, S. Zereshki, and Y. Mansourpanah, Preparation and characterization of modified nano-porous PVDF membrane with high antifouling property using UV photo-grafting, Appl. Surf. Sci. 255 (2009) 7455–7461.

[76] A. Ghaee, A. Ghadimi, B. Sadatnia, A.F. Ismail, Z. Mansourpour and M. Khosravi, Synthesis and characterization of poly(vinylidene fluoride) membrane containing hydrophobic silica nanoparticles for $CO_2$ absorption from $CO_2/N_2$ using membrane contactor, Chem. Eng. Res. Des. 120 (2017) 47-57.

[77] F. Liu, B.K. Zhu, and Y.Y. Xu, Improving the hydrophilicity of poly(vinylidene fluoride) porous membranes by electron beam initiated surface grafting of AA/SSS binary monomers, Appl. Surf. Sci. 253 (2006) 2096–2101.

[78] D. L. Pavia, G. M. Lampman, and G. S. Kriz, Introduction to Spectroscopy: a guide for students of organic chemistry, 2009.

[79] Y. Sui, Z. Wang, C. Gao, Q. Wana, and L. Zhu, An investigation on the antifouling ability of PVDF membranes by polyDOPA coating, Desalin. Water Treat. 50 (2012) 22–33.

[80] F. Wu, J. Li, K. Zhang, Z. He, P. Yang, D. Zou, N. Huang, Multifunctional Coating Based on Hyaluronic Acid and Dopamine Conjugate for Potential Application on Surface Modification of Cardiovascular Implanted Devices, ACS Appl. Mater. Interfaces 8 (2016) 109–121.

[81] B. Xu, Y. Liu, L.Wang, X. Ge, M. Fu, P. Wang, Q. Wang, High-Strength Nanocomposite Hydrogels with Swelling-Resistant and Anti-Dehydration Properties, Polymers (Basel)., vol. 10, no. 9, p. 1025, 2018.

[82] H. S. Rabbani, V. Joekar-Niasar, and N. Shokri, Effects of intermediate wettability on entry capillary pressure in angular pores, J. Colloid Interf. Sci. 473 (2007) 34–43.

[83] E. E. Meyer, K. J. Rosenberg, and J. Israelachvili, Recent progress in understanding hydrophobic interactions, Proc. Natl. Acad. Sci. 103 (2006) 15739–15746.

[84] F. Martínez, "Physics and Chemistry of Liquids", pp. 686–702, 2016.

[85] K.T. Savjani, A.K. Gajjar and J.K. Savjani, Drug Solubility: Importance and Enhancement Techniques, ISRN Pharmaceutics. (2012) 195727.

[86] W. L. Hough, M. Smiglak, H. Rodríguez, R. P. Swatloski, S. K. Spear, D. T. Daly, J. Pernak, J. E. Grisel, R. D. Carliss, M. D. Soutullo, Jr. Davis, H. James, R. D. Rogers, The third evolution of ionic liquids: active pharmaceutical ingredients, New J. Chem. 31 (2007) 1429-1436.

[87] P. Kogner, J. L. Johnsen, M. Lindskog, F. Ponthan, L. Elfman, A. Orrego, B. Sveinbjörnsson, "Cyclooxygenase-2 Is Expressed in Neuroblastoma, and Nonsteroidal Anti-Inflammatory Drugs Induce Apoptosis and Inhibit Tumor Growth In vivo, Cancer Res. 64, (2005) 7210–7215.

[88] A. Livingston, Mechanism of Action of Nonsteroidal Anti-Inflammatory Drugs, Vet. Clin. North Am. Small Anim. Pract. 30 (2000) 773–781.

[89] B. Cryer and M. Feldman, Selectivity of Widely Used Nonsteroidal Anti-Inflammatory Drugs, Am. J. Med. 104 (1998) 413–421.

[90] J .R. Vane and R. M. Botting, "Mechanism of Action of Nonsteroidal Anti-inflammatory Drugs", Am. J. Med. 104 (1998) 2S–8S.

[91] G. D. Krischak, P. Augat, L. Claes, L. Kinzl, and A. Beck, The effects of non-steroidal anti-inflammatory drug application on incisional wound healing in rats, J. Wound Care 16 (2007) 76–78.

[92] K.D. Nguyen and D.A. Lee, In Vitro Evaluation of Antiproliferative Potential of Topical Cyclo-oxygenase Inhibitors in Human Tenon's Fibroblasts, Exp. Eye Res. 57 (1993) 97–105.

[93] J. Martinez, T. Sancheza and J.J. Moreno, Role of prostaglandin H synthase-2-mediated conversion of arachidonic acid in controlling 3T6 fibroblast growth, Am. J. Physiol. Physiol. 273 (1997) 1466–1471.

[94] W. Miltyk, E. Karna and J. Pałka, Inhibition of prolidase activity by non-steroid antiinflammatory drugs in cultured human skin fibroblasts., Pol. J. Pharmacol. 48 (n.d.) 609–13.

[95] A. Surazyński, J. Pałka and S. Wołczyński, Acetylsalicylic acid-dependent inhibition of collagen biosynthesis and beta1-integrin signaling in cultured fibroblasts., Med. Sci. Monit. 10 (2004).

[96] R.D. Price, S. Myers, I.M. Leigh and H.A. Navsaria, The Role of Hyaluronic Acid in Wound Healing, Am. J. Clin. Dermatol. 6 (2005) 393–402.

[97] F. Yin, L. Lin, S. Zhan, Preparation and properties of cellulose nanocrystals, gelatin, hyaluronic acid composite hydrogel as wound dressing, J. Biomater. Sci. Polym. Ed. 30 (2019) 190–201.

[98] N. Karimi Dehkordi, M. Minaiyan, A. Talebi, V. Akbari and A. Taheri, Nanocrystalline cellulose–hyaluronic acid composite enriched with GM-CSF loaded chitosan nanoparticles for enhanced wound healing, Biomed. Mater. 14 (2019) 035003.

[99] J.K. Kutty, E. Cho, J. Soo Lee, N.R. Vyavahare and K. Webb, The effect of hyaluronic acid incorporation on fibroblast spreading and proliferation within PEG-diacrylate based semi-interpenetrating networks., Biomaterials. 28 (2007) 4928–38.

**Graphical abstract**